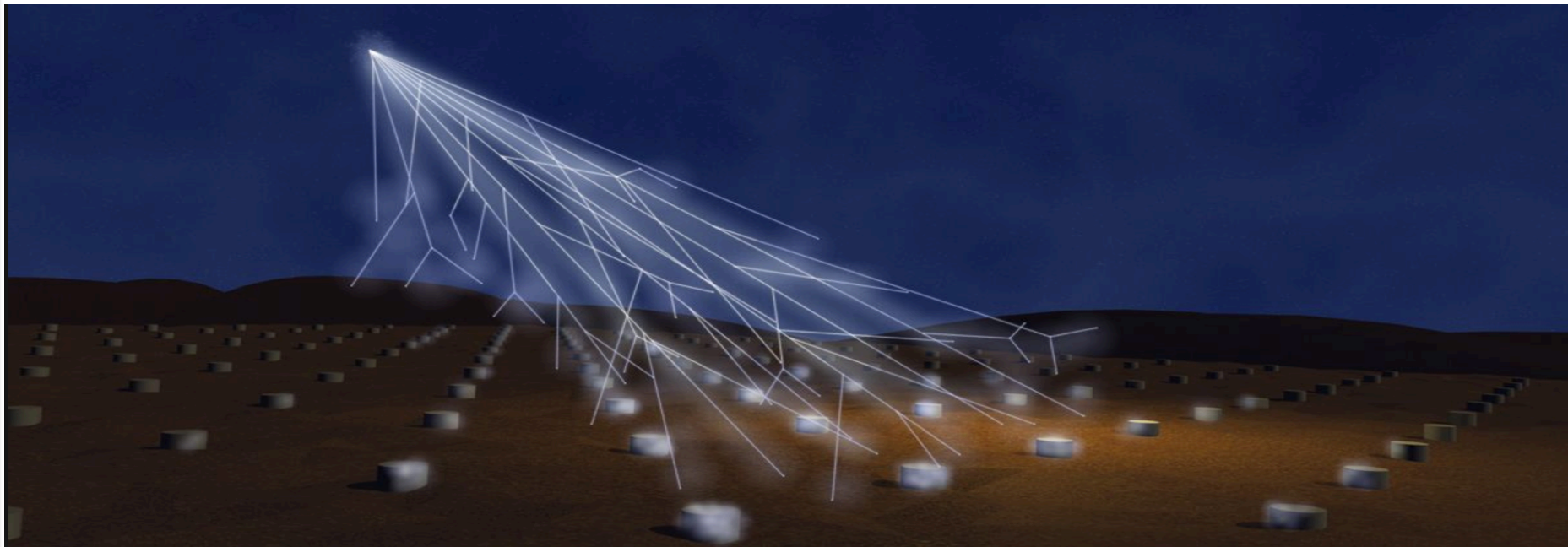


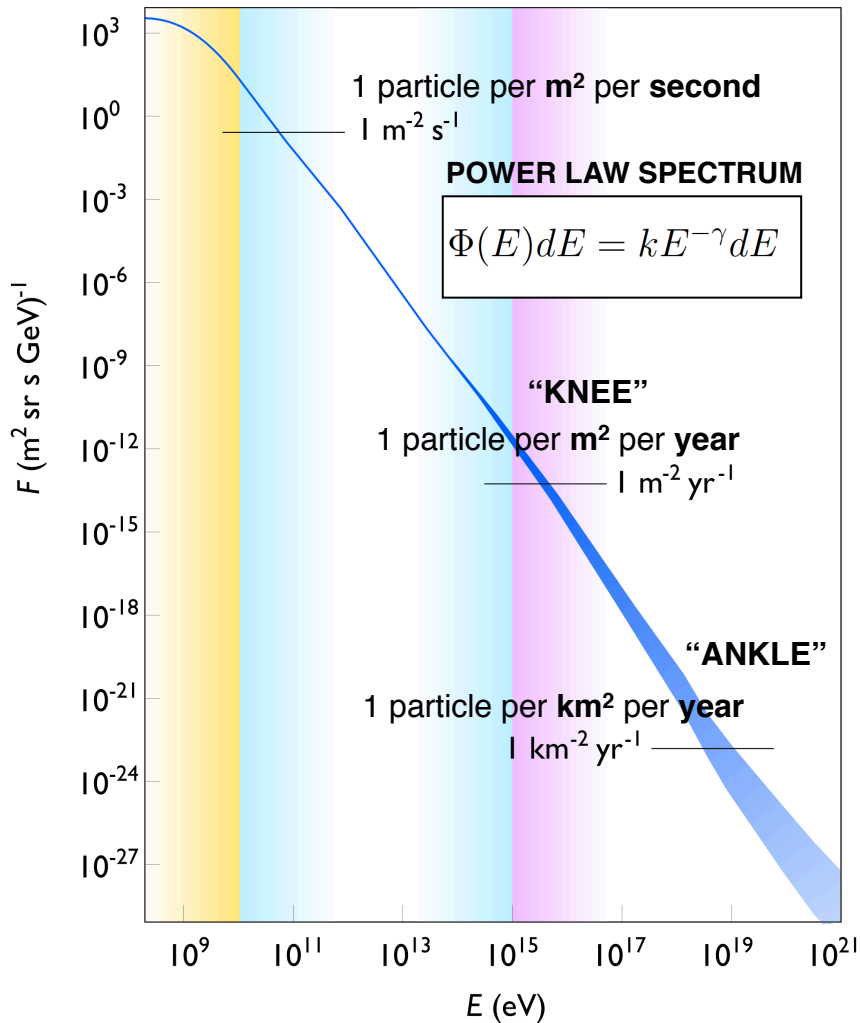
Cosmic ray indirect detection

Lez 21bis 191219

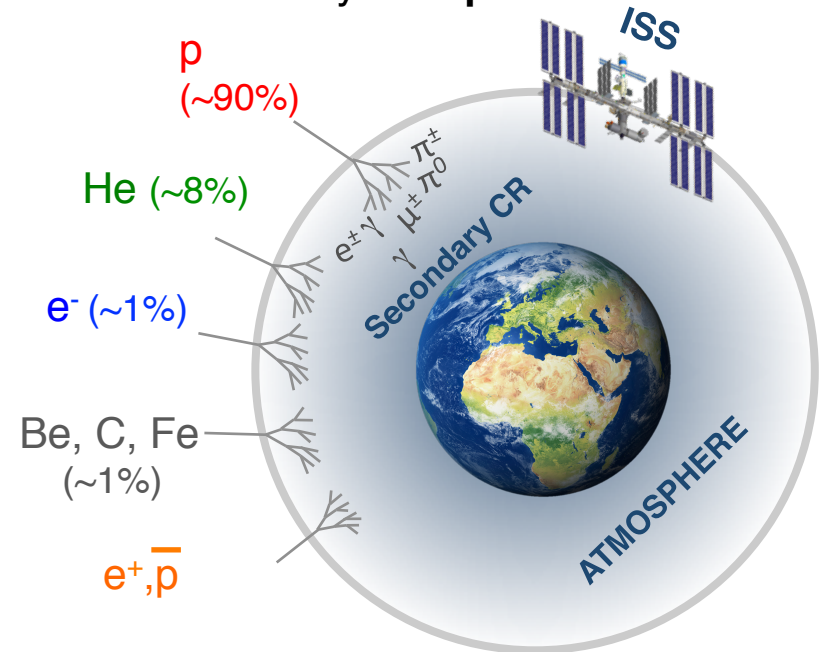


Cosmic Rays

Cosmic ray flux at Earth

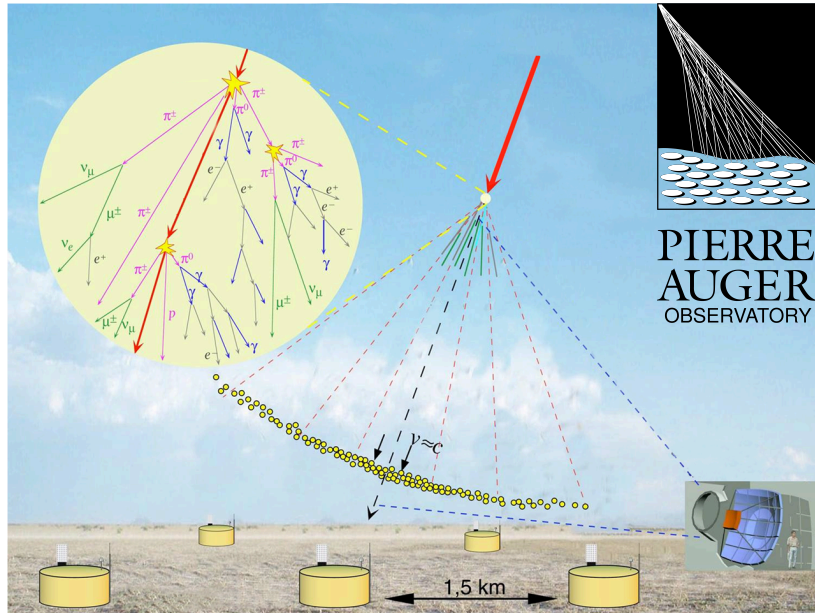


- Cosmic ray Flux: Intensity of CR in space per **unit of area, solid angle, time and energy**
- Energy range up to **10^{20} eV**
- Intensities spanning **30 orders of magnitude**
- Most of cosmic rays are **protons and nuclei**

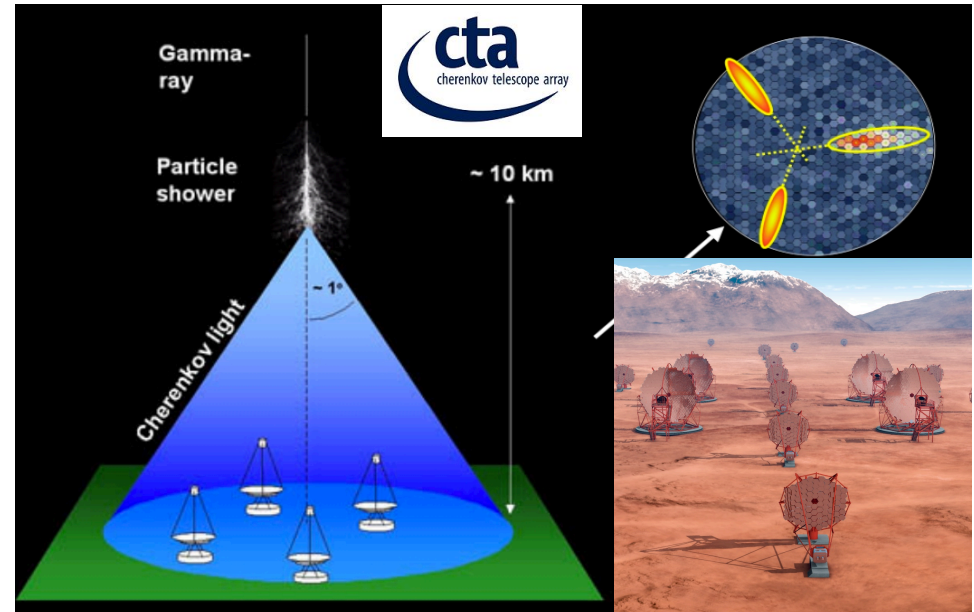


Ground based experiments

Charged CRs



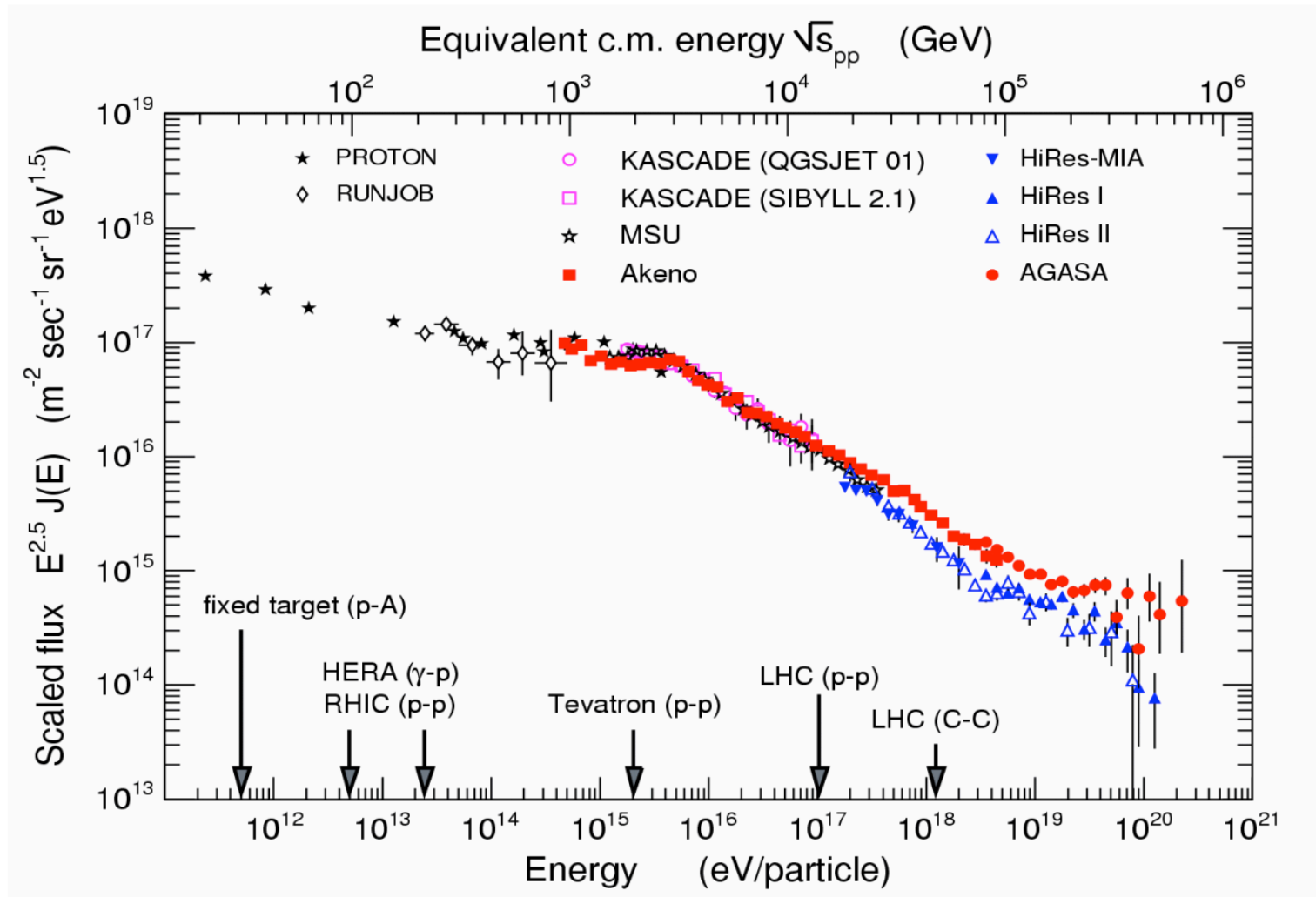
Gamma Rays



- ✓ Large collection areas → probe CR energies TeV –Eev ranges
- ✗ Indirect measurements
 - Primary CR identified via the analysis of shower shapes and composition at ground (highly rely on MonteCarlo simulations)
 - Main systematics are the parametrization of X-sections at very high energies

The ultra-high-energy flux

Cosmic ray flux and energy scales



The indirect measurement principle

- When high energy cosmic rays enter the atmosphere, they initiate **particle showers**. Secondary particles may reach the ground and be detected by ground experiments. **The atmosphere is used as a huge calorimeter.**
- High energy CR fluxes are faint, so we need **large (up to $O(1000)$ km²) collection areas** to maximize the statistics.
- The primary particle properties is inferred from the properties of the shower sampled at ground. **Indirect measurements are characterized by uncertainties with are typically one order of magnitude worse than direct detection experiments.**

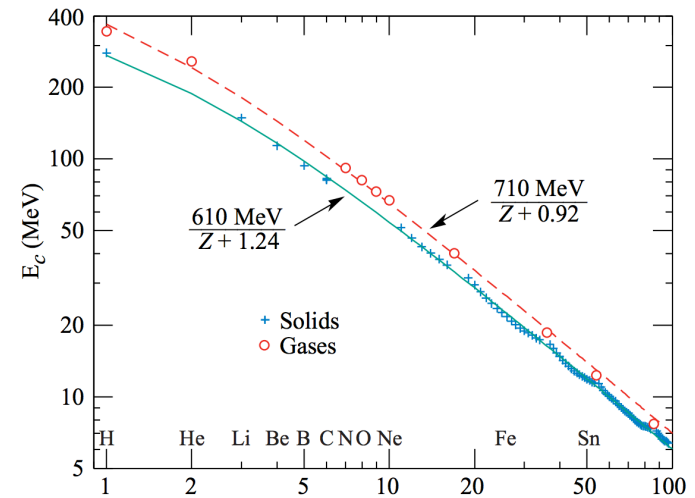
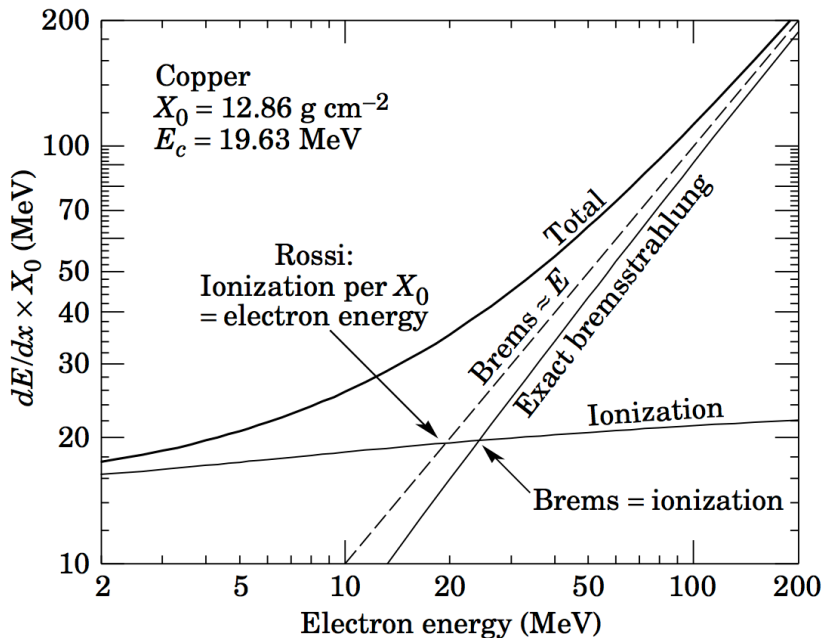
The indirect measurement principle

The Pierre Auger Observatory in Umbria



Particle showers

- Electromagnetic shower development is defined by the interactions in matter of high energy photons and electrons



Material		X_0 (g cm ⁻²)	λ_I (g cm ⁻²)	E_c (MeV)
Active detectors	NaI	9.5	151	12.5
	BGO	8.0	157	7
Passive absorbers	Fe	13.8	132	28
	Pb	6.4	194	9.5
	U	6.0	199	9
Air [STP]	Mixture	36.7	90	86

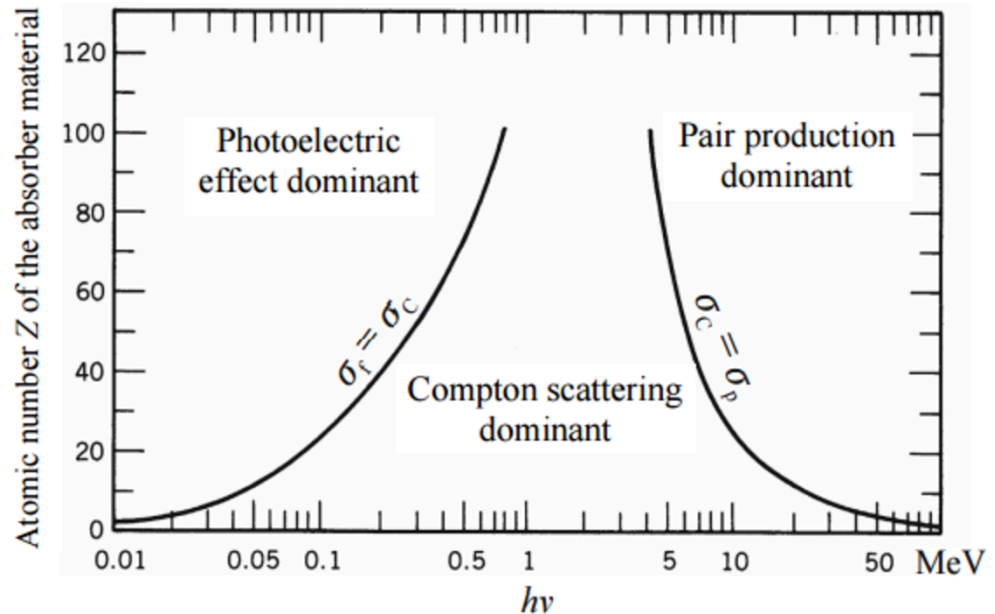
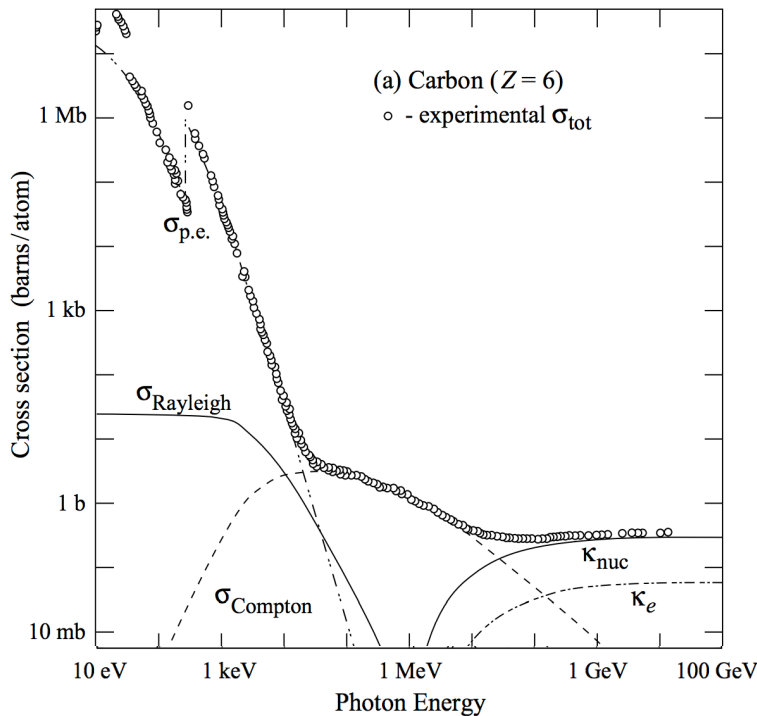
Critical energy for electrons in air $\sim 100 \text{ MeV}$ (for muons $E_c(\mu) = (m_\mu/m_e)^2 E_c(e)$)

Interaction length for electrons in air $\sim 30 \text{ g/cm}^2$

Above critical energy, electrons loose energy via Bremsstrahlung. Below, they ionize.

Particle showers

- Electromagnetic shower development are defined by the interactions in matter of high energy photons and electrons



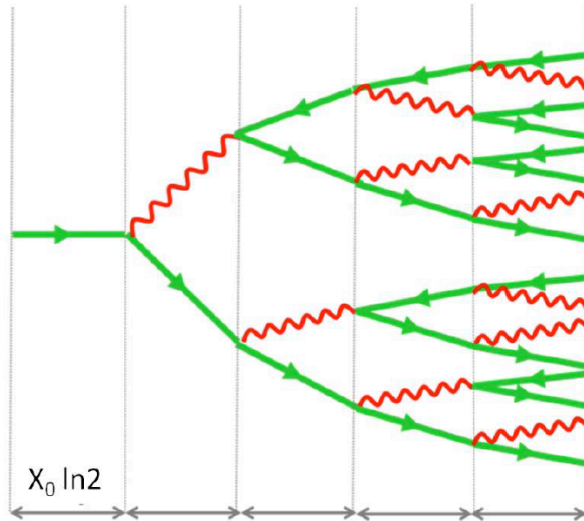
$$X_0 (\text{p.p.}) = 9/7 X_0 (\text{Bremms})$$

Above critical energy, photons convert in e^+e^- with a typical length of X_0 (p.p.)

$$I(x) = I(0) \exp(-X/X_0)$$

Particle showers

- The Heitler/Rossi model can be used to understand the basic properties of electromagnetic showers



The electron losses half of his energy when :

$$R = X_0 \ln(2)$$

Define the scale variables:

$$t = z/X_0 \quad y = E_0/E_c$$

Total number of produced electrons after $z = n R$: $N(z) = 2^n$

Mean energy for each particle :

$$E(z) = E_0/2^n$$

Particle creation in shower stops when $E < E_c$:

$$n_c = \frac{1}{\ln 2} \ln \left(\frac{E_0}{E_c} \right)$$

Maximum depth :

$$z_{max} = X_0 \ln \left(\frac{E_0}{E_c} \right)$$

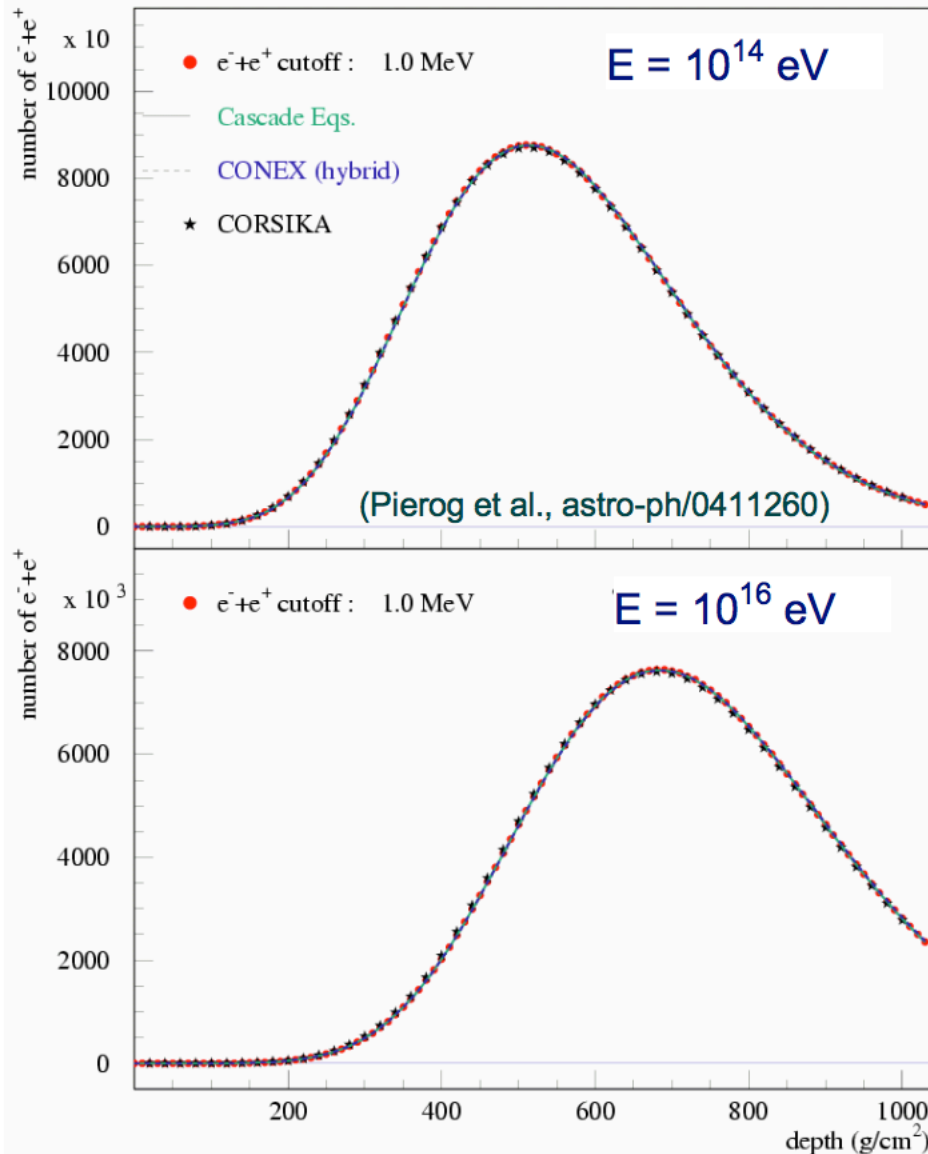
Numer of particle at z_{max} :

$$N_{max} = E_0/E_c$$

d=	1	2	3	4	5
N=	2	4	8	16	32
E=	1/2	1/4	1/8	1/16	1/32

Fig. 4.2. Toy model evolution of an electromagnetic cascade. At each step of the cascade the number of particles is multiplied by two, through either pair creation or single photon bremsstrahlung. Backward arrows indicate a positron, as in Feynman diagrams. The evolution stops when individual particle energies fall below the critical energy E_c . The number N of particles at each step d and the average particle energy E in the Heitler's model are also indicated. Adapted from [4ww01]

Particle showers



Electromagnetic shower can be well modelled using semi-analytical parametrizations or MonteCarlo simulations

Atmosphere

Altitude (km)	Vertical depth (g/cm ²)	Local density (10 ⁻³ g/cm ³)	Molière unit (m)	Electron Cherenkov threshold (MeV)	Cherenkov angle (°)
40	3	3.8×10^{-3}	2.4×10^4	386	0.076
30	11.8	1.8×10^{-2}	5.1×10^3	176	0.17
20	55.8	8.8×10^{-2}	1.0×10^3	80	0.36
15	123	0.19	478	54	0.54
10	269	0.42	223	37	0.79
5	550	0.74	126	28	1.05
3	715	0.91	102	25	1.17
1.5	862	1.06	88	23	1.26
0.5	974	1.17	79	22	1.33
0	1,032	1.23	76	21	1.36

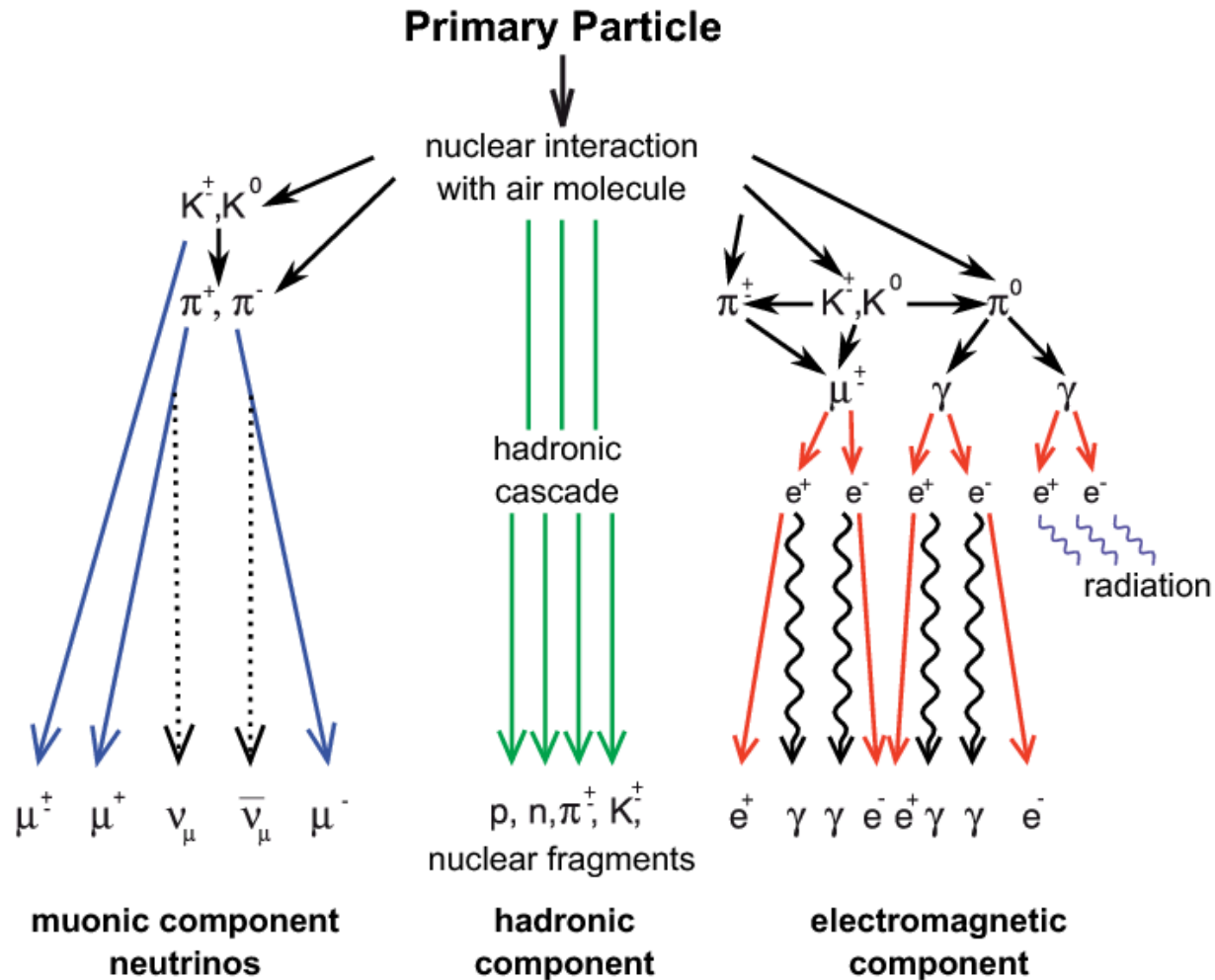
Critical energy: $E_c = \alpha X_0 \sim 85 \text{ MeV}$

Radiation length: $X_0 \sim 36 \text{ g/cm}^2$

Total atmosphere depth = c.a. 1000 g/cm²

Particle showers

- Showers initiated by **hadronic interactions**



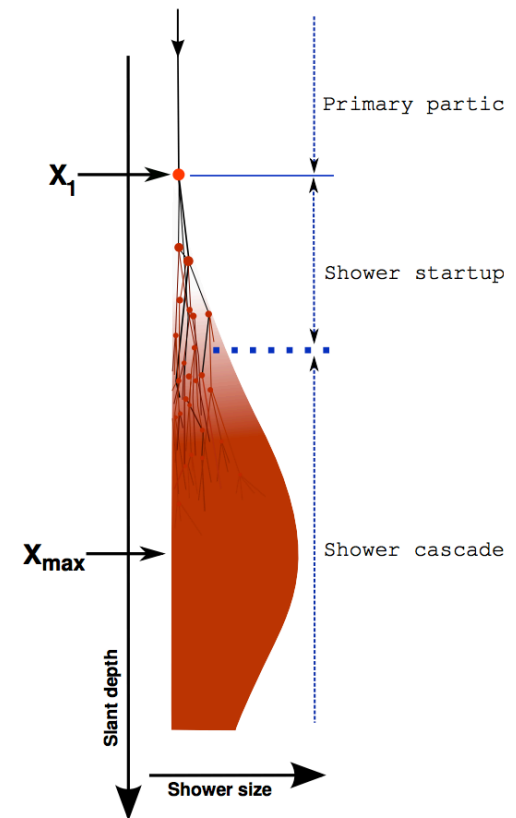
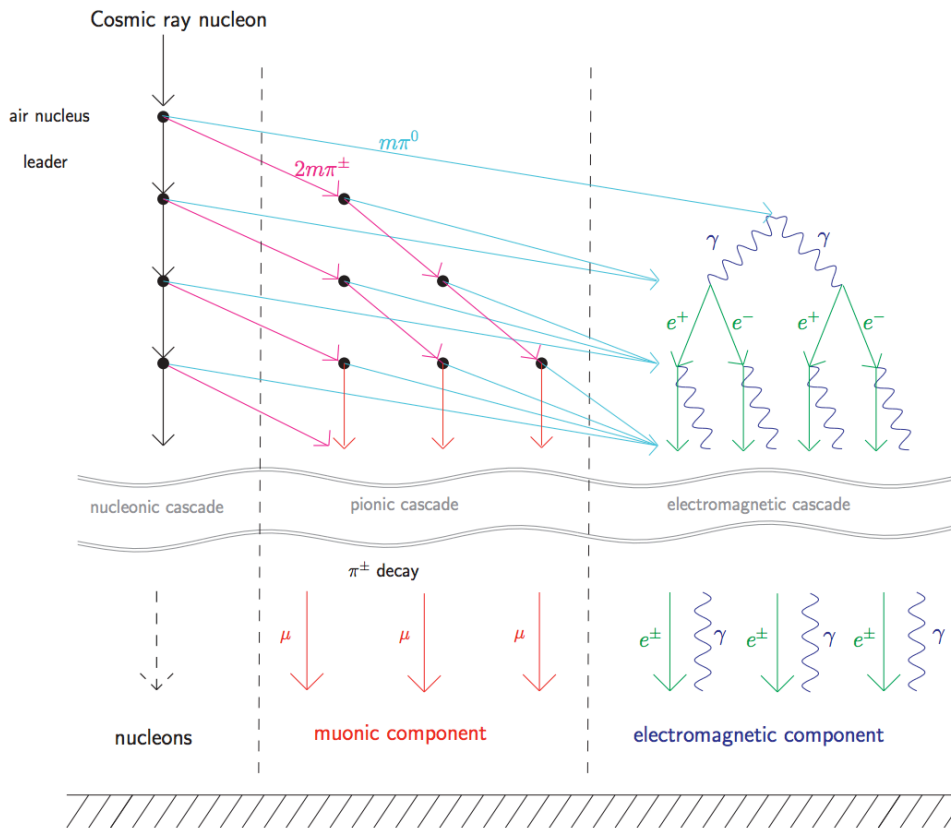
Particle showers

$p + N \longrightarrow \pi^{\pm}, \pi^0, K^{\pm}, K, p, n, +\dots(\text{exotic})$ strong int.

$\pi^0 \longrightarrow \gamma\gamma$ $\tau_{\pi} = 1.8 \cdot 10^{-16} s$ e.m. int.

$\pi^{\pm} \longrightarrow \mu^{\pm} \nu_{\mu}$ $\tau_{\pi} = 2.5 \cdot 10^{-8} s$ weak int.

$\mu^{\pm} \longrightarrow e^{\pm} \nu_e \nu_{\mu}$ $\tau_{\mu} = 2.2 \cdot 10^{-6} s$ weak int.



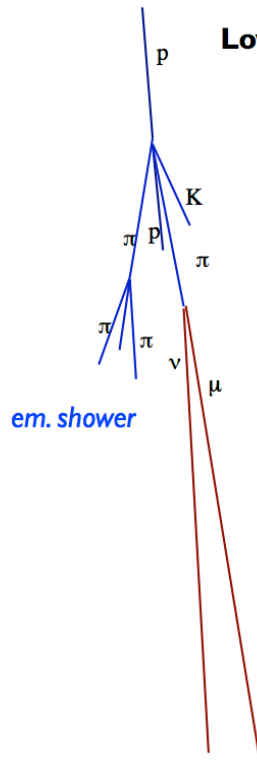
Particle showers

$p + N \longrightarrow \pi^\pm, \pi^0, K^\pm, K, p, n, +\dots(\text{exotic})$ strong int.

$\pi^0 \longrightarrow \gamma\gamma$ $\tau_\pi = 1.8 \cdot 10^{-16} s$ e.m. int.

$\pi^\pm \longrightarrow \mu^\pm \nu_\mu$ $\tau_\pi = 2.5 \cdot 10^{-8} s$ weak int.

$\mu^\pm \longrightarrow e^\pm \nu_e \nu_\mu$ $\tau_\pi = 2.2 \cdot 10^{-6} s$ weak int.

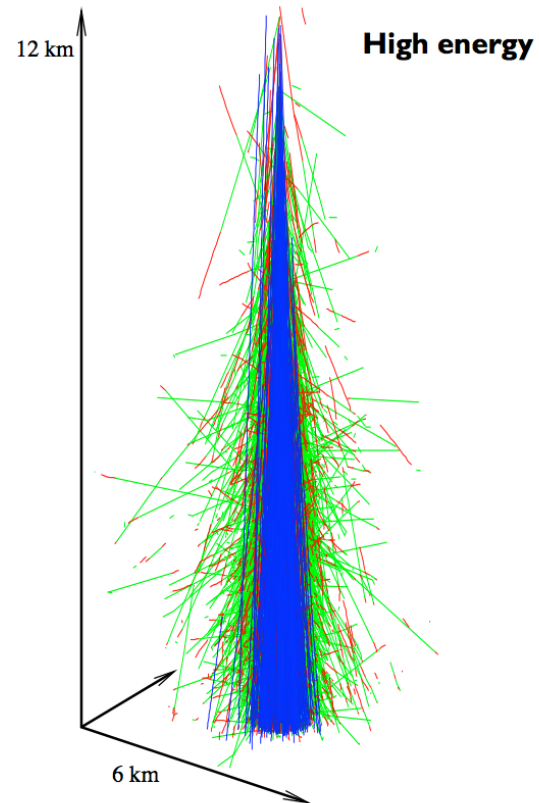


Typical energies above which particles interact

$$E_{\pi^\pm} \sim 30 \text{ GeV}$$

$$E_K \sim 200 \text{ GeV}$$

$$E_{\pi^0} \sim 10^{19} \text{ eV}$$



Particle showers

$$p + N \longrightarrow \pi^{\pm}, \pi^0, K^{\pm}, K, p, n, + \dots (\text{exotic})$$

$$\pi^0 \longrightarrow \gamma\gamma \quad \tau_{\pi} = 1.8 \cdot 10^{-16} s$$

$$\pi^{\pm} \longrightarrow \mu^{\pm} \nu_{\mu} \quad \tau_{\pi} = 2.5 \cdot 10^{-8} s$$

$$\mu^{\pm} \longrightarrow e^{\pm} \nu_e \nu_{\mu} \quad \tau_{\mu} = 2.2 \cdot 10^{-6} s$$

Hadronic shower dynamics can be understood using a “simplicistic” model.

- After each interaction, the primary nucleon carries a fraction **1-f (inelasticity)** of its initial energy E_0 , and the rest f is distributed to the N_{π} pions.
- The multiplicity N_{π} is a function of \sqrt{s} , and $N_{\pi+/-} \sim E^{0.2}$ (from lab measurements, $N_{\pi+/-} = 10$ for $E_0 = 100 \text{ GeV}$)
- After k interactions, the primary carries $(1-f)^k E_0$ energy. The rest is spread among N_{π} pions, each having energy around $E_0 / (N_{\pi})^k$
- **π_0 decay instantly, transferring their energy to the electromagnetic component of the shower**
- **$\pi^{+/-}$ decay slower, and the decay probability concurs with the interaction probability.** If $E_{\pi} > E_{\pi}^{\text{crit}} \sim 20 \text{ GeV}$, pions continue to interact. Otherwise, they decay transferring their energy to the muonic and invisible component of the shower

Particle showers

$$p + N \longrightarrow \pi^{\pm}, \pi^0, K^{\pm}, K, p, n, + \dots (\text{exotic})$$

$$\pi^0 \longrightarrow \gamma\gamma \quad \tau_{\pi} = 1.8 \cdot 10^{-16} \text{ s}$$

$$\pi^{\pm} \longrightarrow \mu^{\pm} \nu_{\mu} \quad \tau_{\pi} = 2.5 \cdot 10^{-8} \text{ s}$$

$$\mu^{\pm} \longrightarrow e^{\pm} \nu_e \nu_{\mu} \quad \tau_{\mu} = 2.2 \cdot 10^{-6} \text{ s}$$

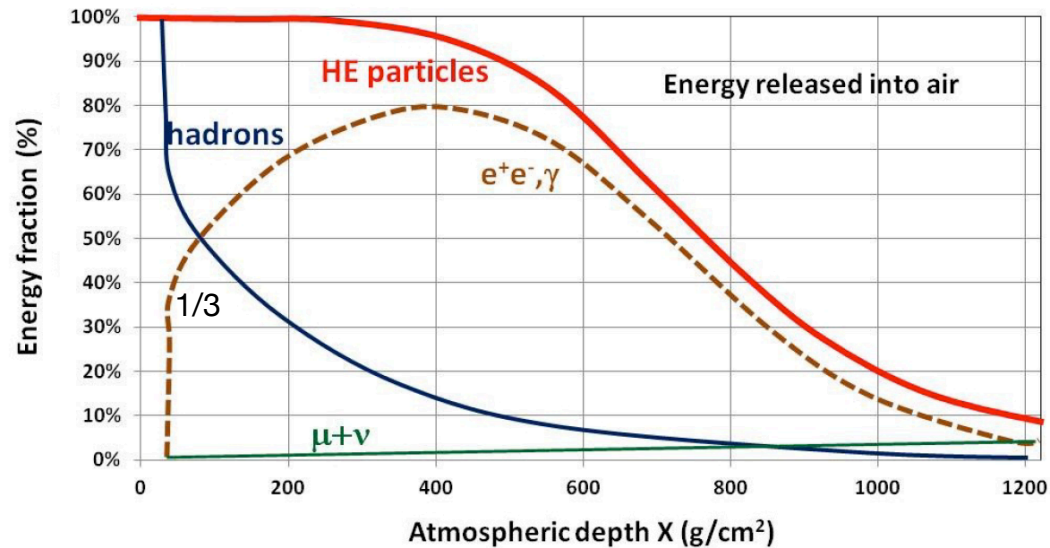


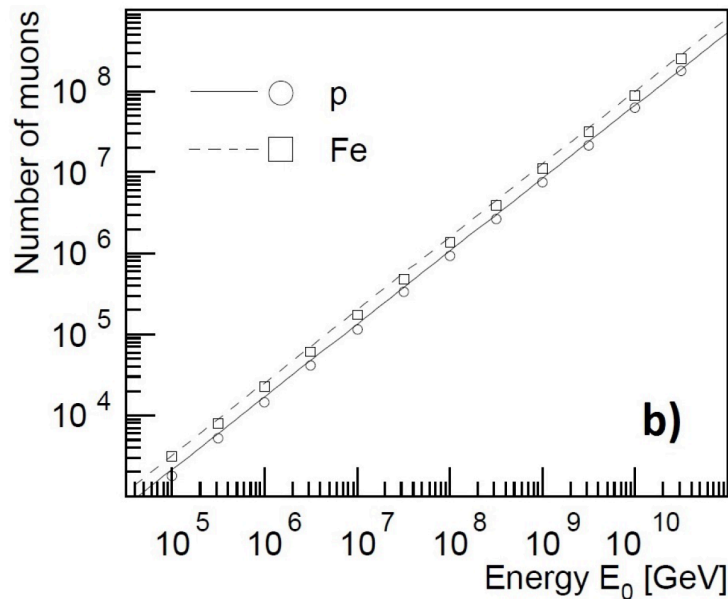
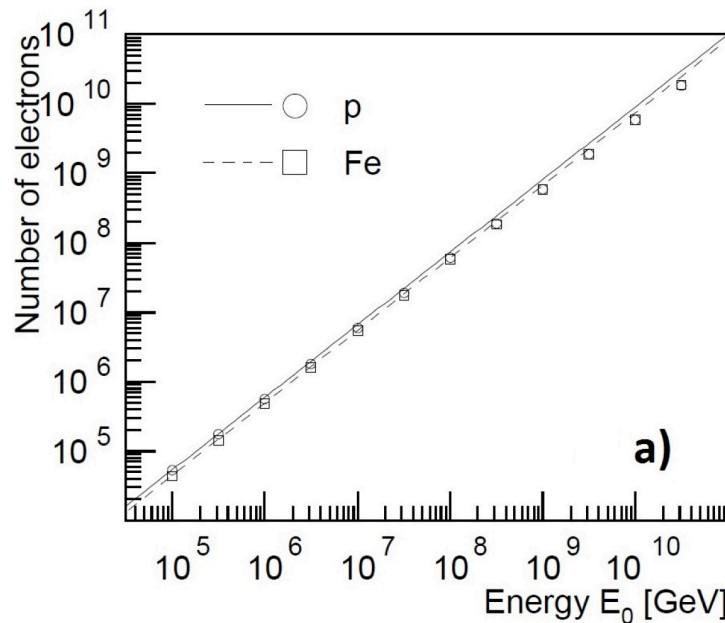
Fig. 4.5. Fraction of energy transferred to the different components of the cascade induced by a primary proton of 10^{19} eV. Part of the energy is released into air by excitation/ionization processes. The top graph uses a linear scale for the energy fraction; the bottom uses a log scale for a better visualization of the “older” part of the shower

Particle showers

- The hadronic shower is a superimposition of em and hadronic sub-showers. The shower maximum for hadr. showers X_{\max} occurs typically higher in the atmosphere than that of em showers with the same energy E_0 , by at least $1.5 \sim 2 X_0$ (energy dependent)
- At ground, we typically measure $e^{+/-}$ below E_c (with $O(10)$ MeV energy), muons with energies 3-4 GeV, and a small fraction of pions, neutrinos.
- The shower dynamics is clearly very complex. However, it has been proved that: the energy of the primary (E_0) can be estimated by measuring the number of electrons (N_e) and muons (N_μ) and it is proportional to a simple function of N_e and N_μ

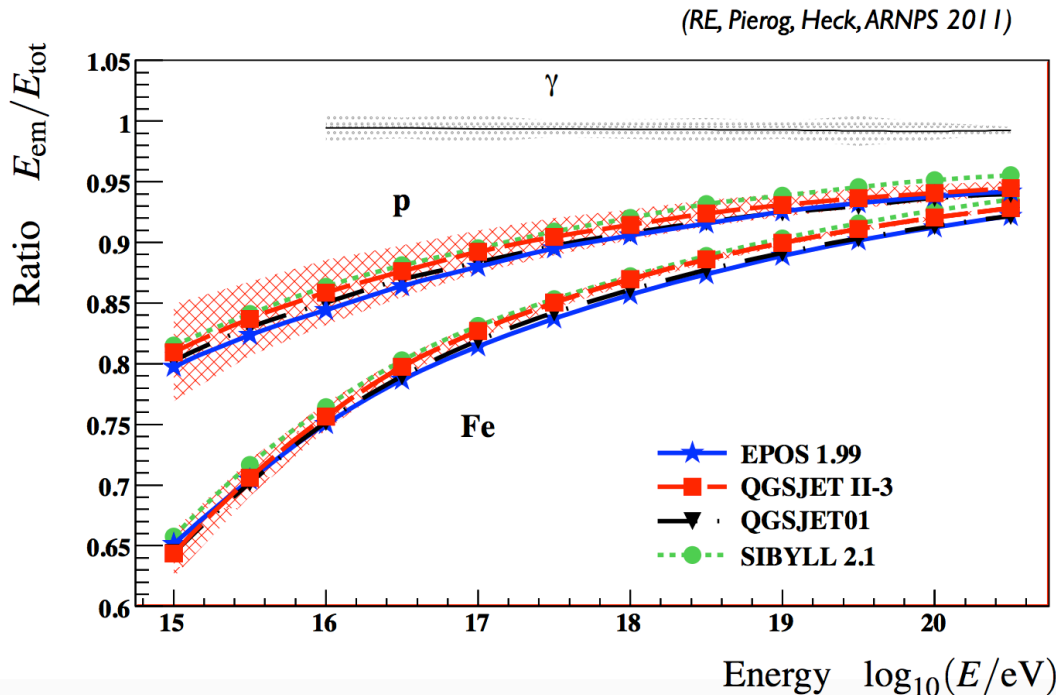
Nuclei-induced showers

- **Superimposition model: the shower induced by a nucleon with mass number A and energy E_0 is equivalent to the superimposition of A showers initiated by $A=1$ (proton) primaries with energy E_0/A .**
- The e.m. content of proton-shower or nuclei-shower is the same. Cannot be used to distinguish them
- The muon content increases slowly as function of A . $N_\mu^{(A)} \sim A^{(1-\beta)} N_\mu^{(p)}$, $(1-\beta) \sim 0.1$



Nuclei-induced showers

- **Superimposition model:** the shower induced by a nucleon with mass number A and energy E_0 is equivalent to the superimposition of A showers initiated by $A=1$ (proton) primaries with energy E_0/A .
- The e.m. content of proton-shower or nuclei-shower is the same. Cannot be used to distinguish them
- The muon content increases slowly as function of A . $N_\mu^{(A)} \sim A^{(1-\beta)} N_\mu^{(p)}$, $(1-\beta) \sim 0.1$



Ratio of e.m. energy content
wrt total shower energy

Nuclei-induced showers

- **Superimposition model:** the shower induced by a nucleon with mass number A and energy E_0 is equivalent to the superimposition of A showers initiated by $A=1$ (proton) primaries with energy E_0/A .
- Nuclei have higher cross-sections, $\sigma \sim A^{2/3}$, so $\lambda^{(A)} \sim A^{-2/3} \lambda^{(p)}$. **Nuclei-induced showers initiate earlier in the atmosphere, with $X_{\max}^{(A)} \sim X_{\max}^{(p)} - X_0 \ln A$**

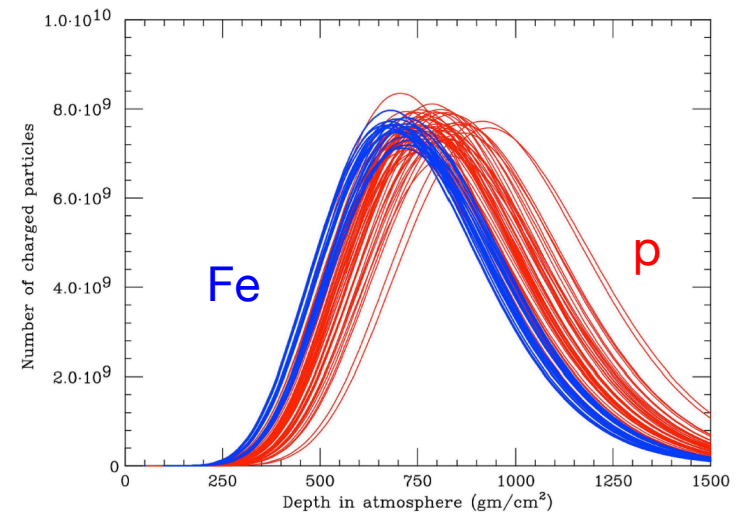
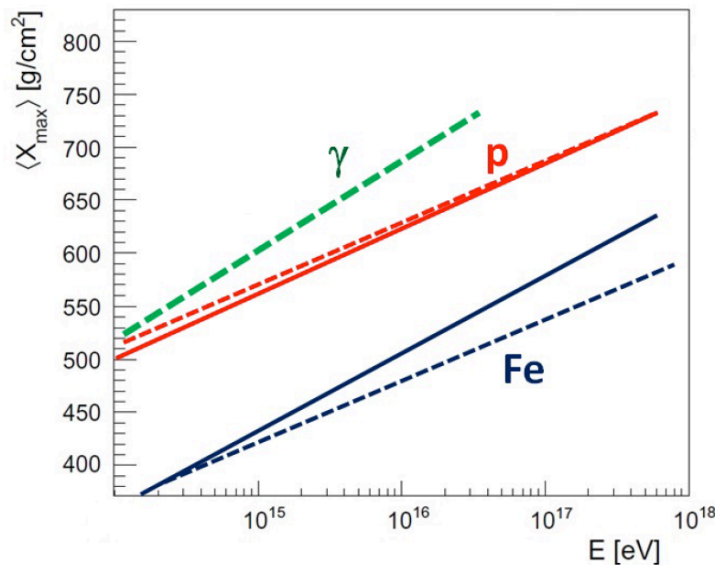
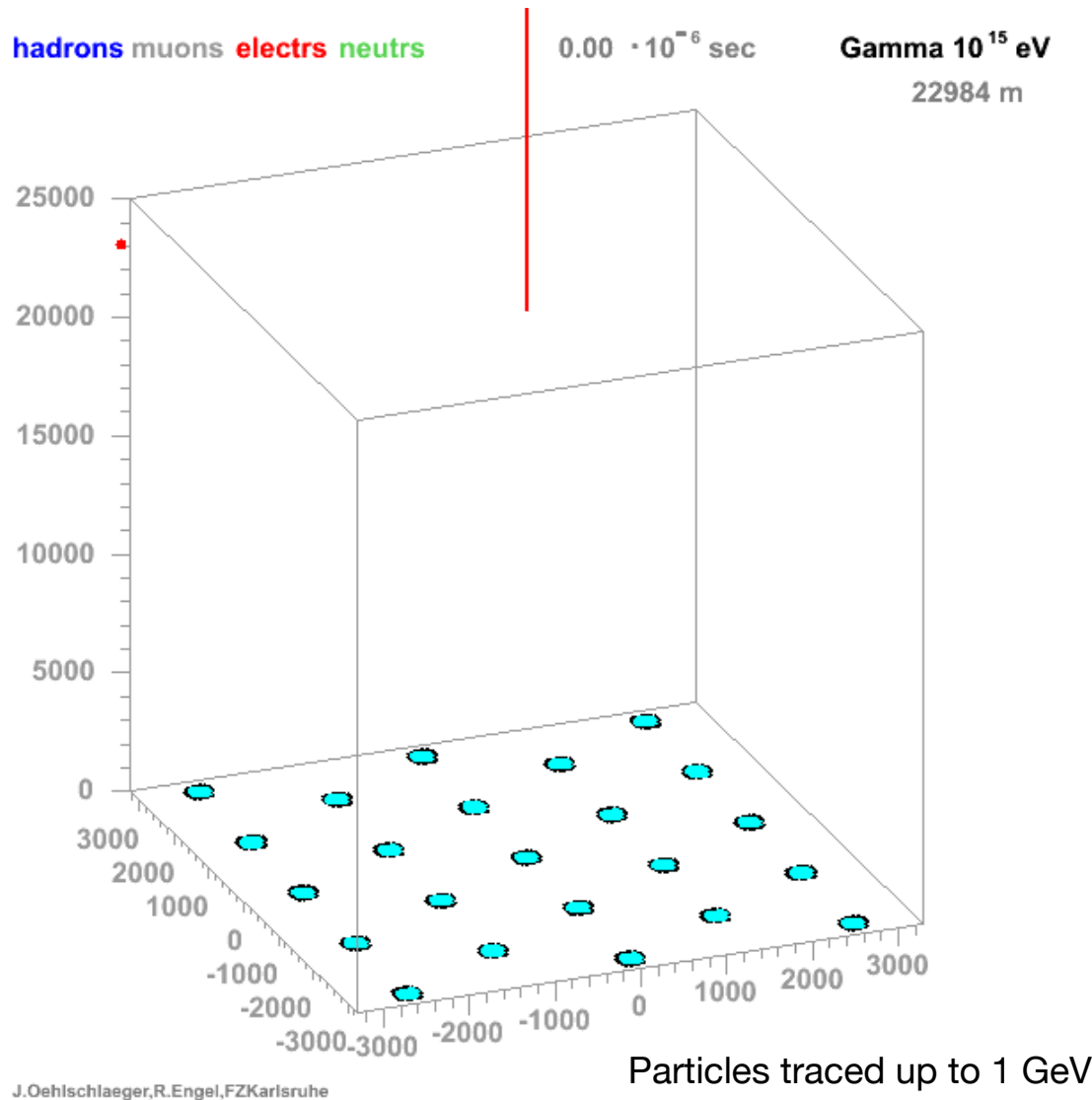
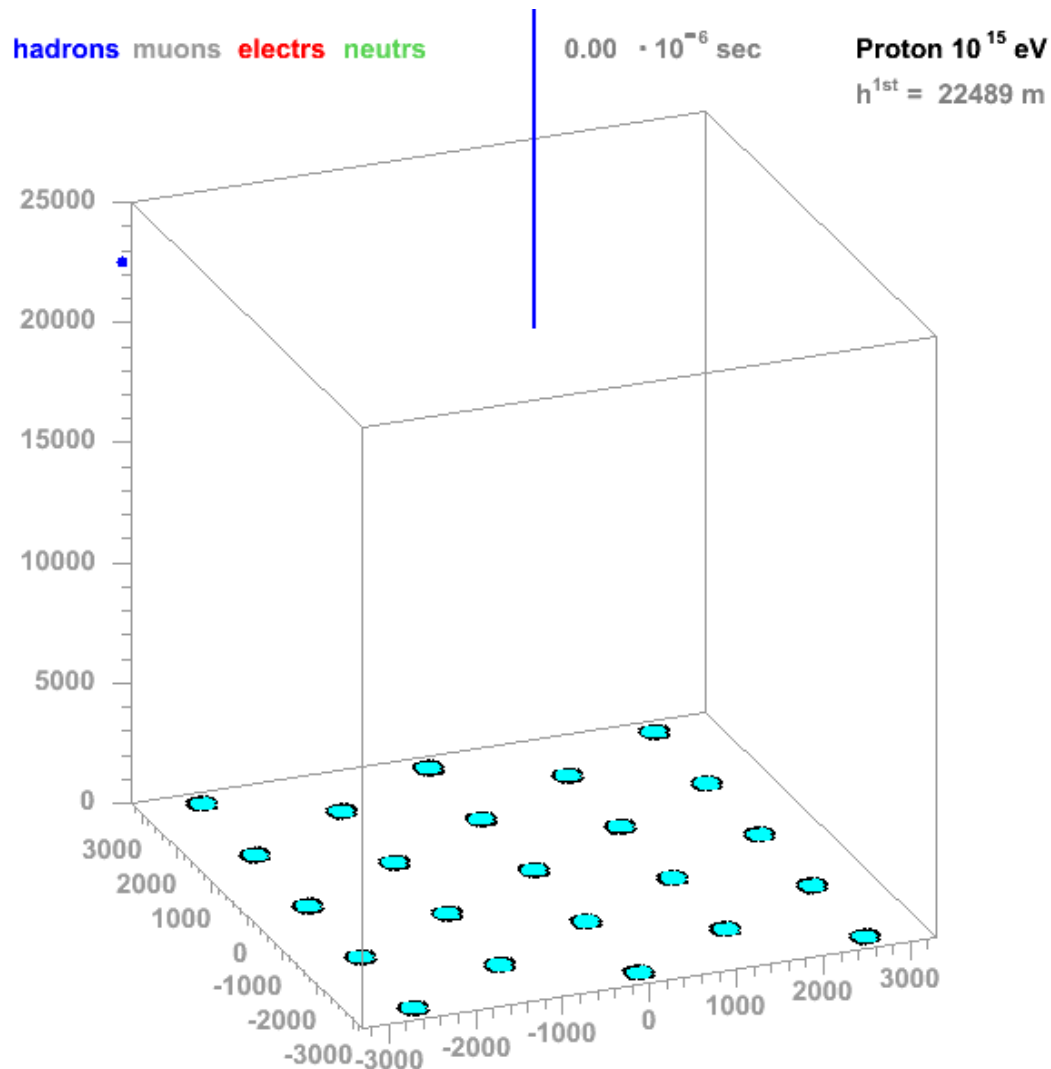


Fig. 4.9. Simulation of the longitudinal profile produced with the CORSIKA code for 50 proton-induced (red) and 50 iron-induced (blue) showers. The same total energy of 10^{19} eV is assumed. Shower-to-shower fluctuations on $N_{e_{\max}}$ and X_{\max} are evident. From [4De08]

Shower numerical simulations



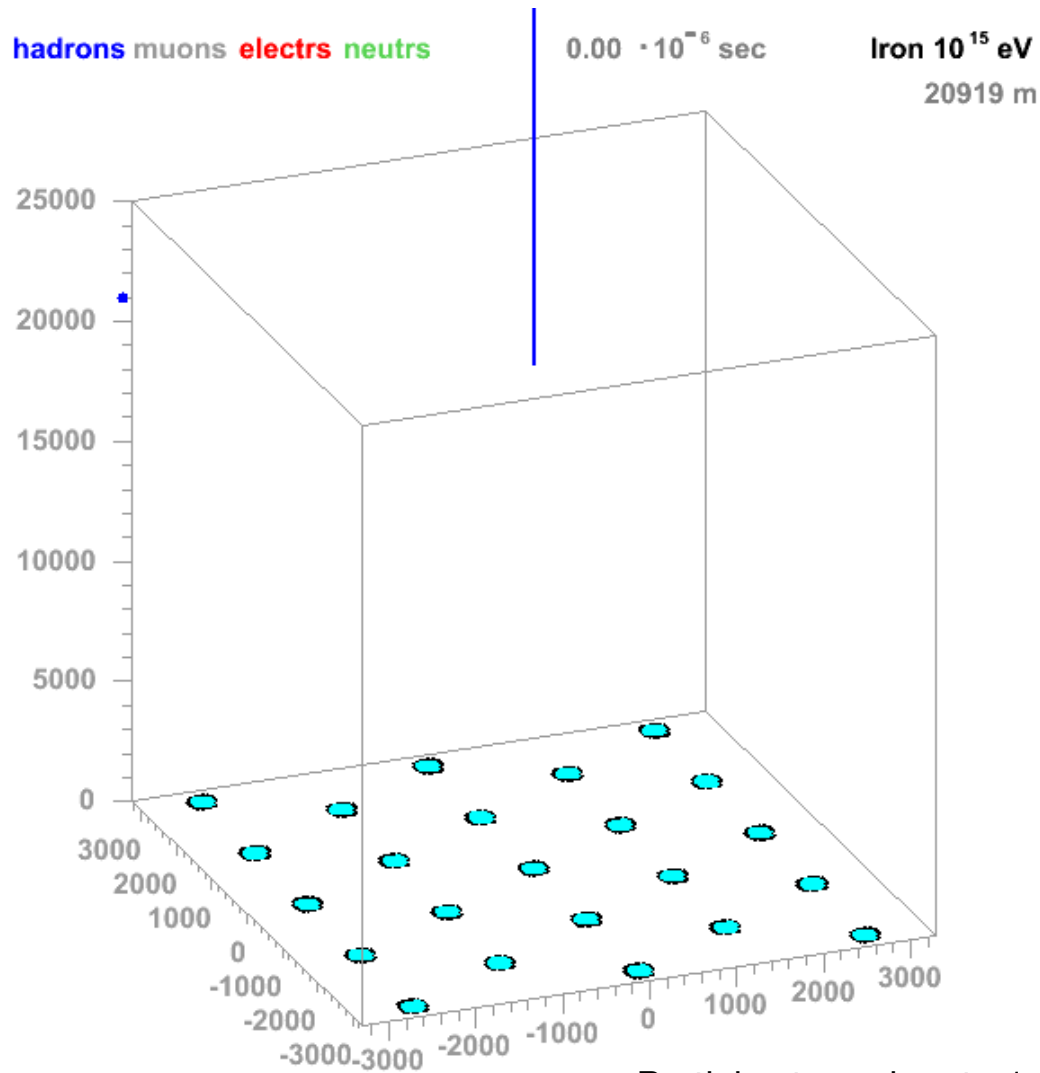
Shower numerical simulations



J.Oehlschlaeger,R.Engel,FZKarlsruhe

Particles traced up to 1 GeV

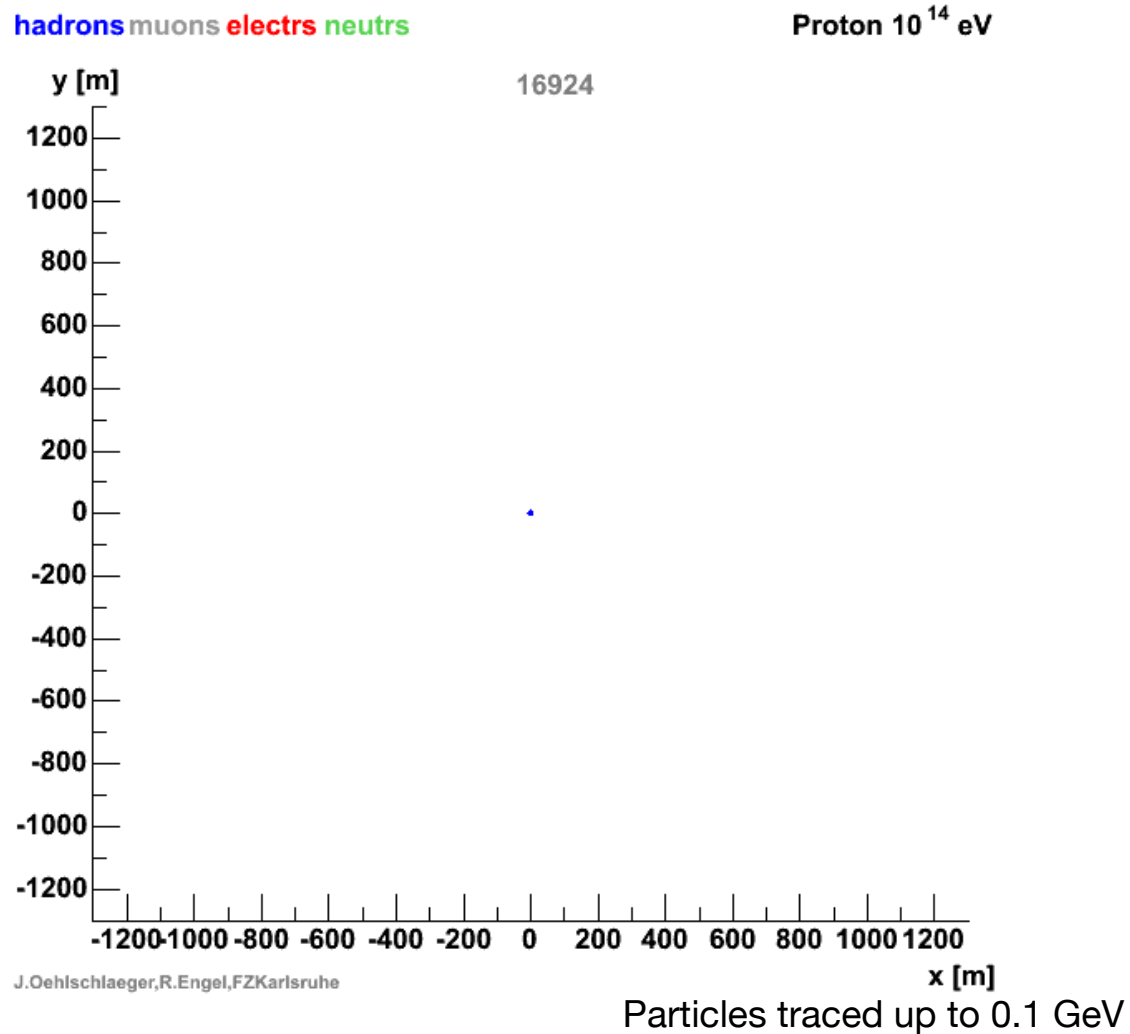
Shower numerical simulations



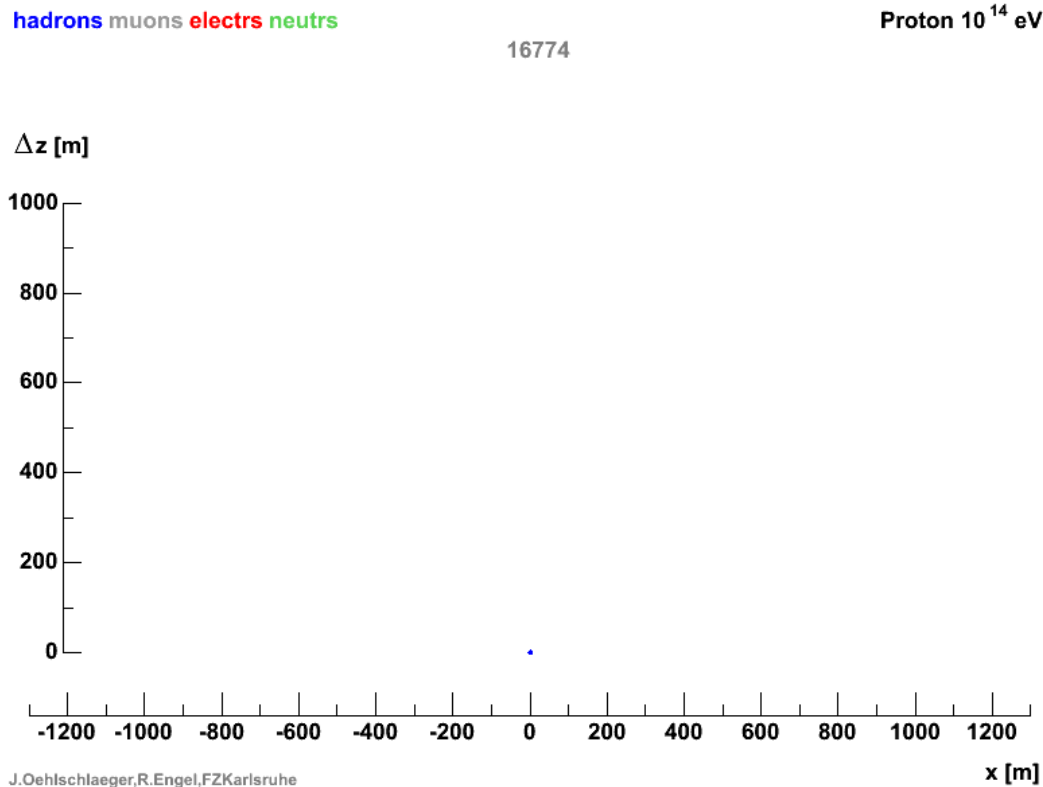
J.Oehlschlaeger,R.Engel,FZKarlsruhe

Particles traced up to 1 GeV

Shower numerical simulations

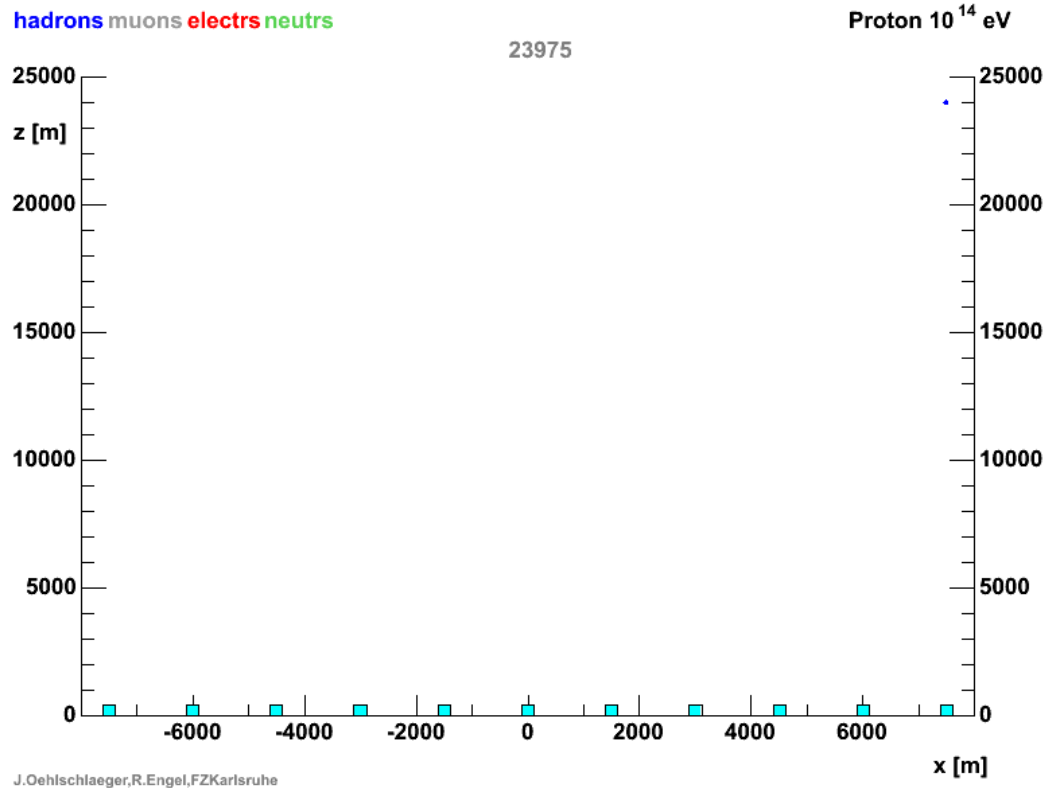


Shower numerical simulations



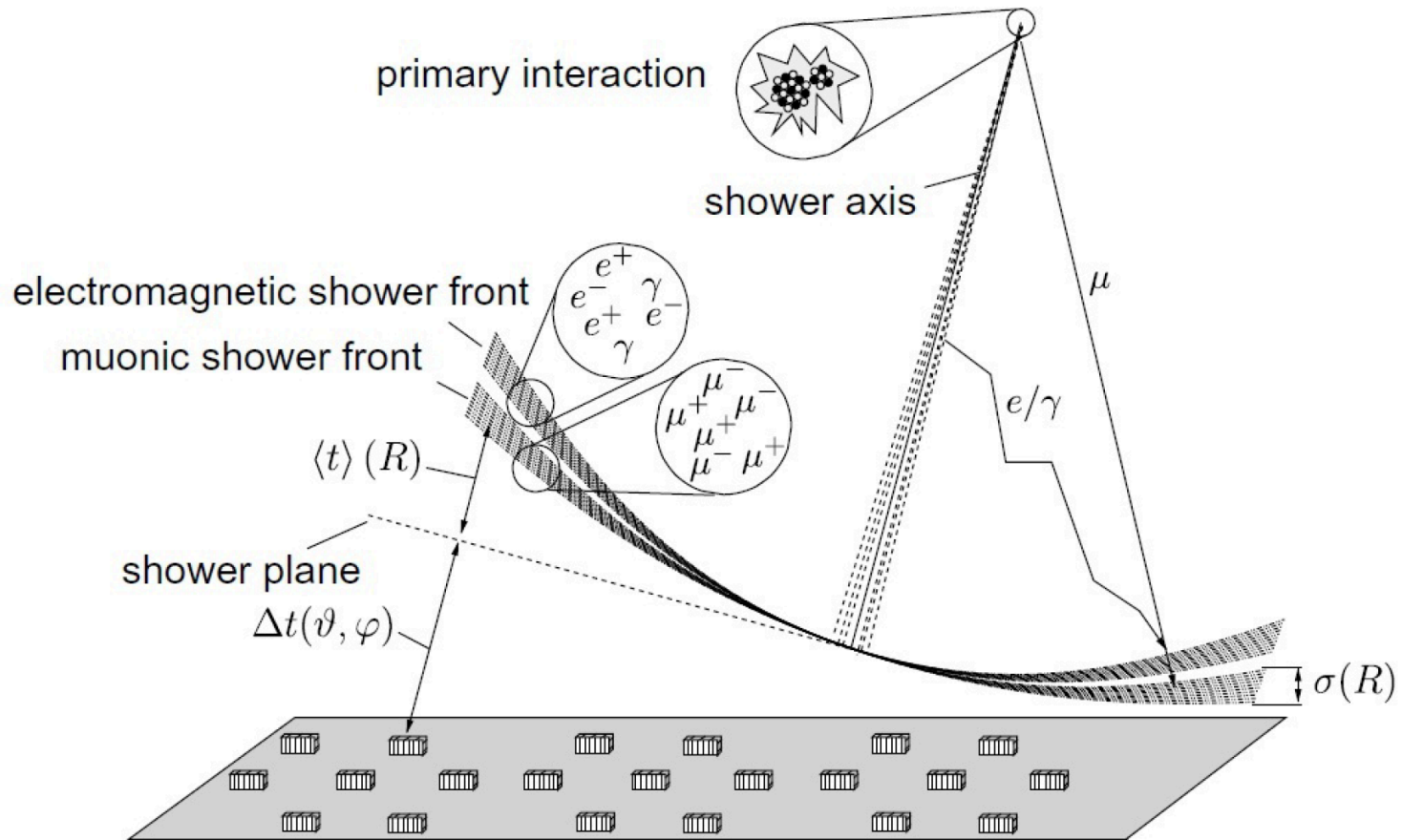
Particles traced up to 0.1 GeV

Shower numerical simulations



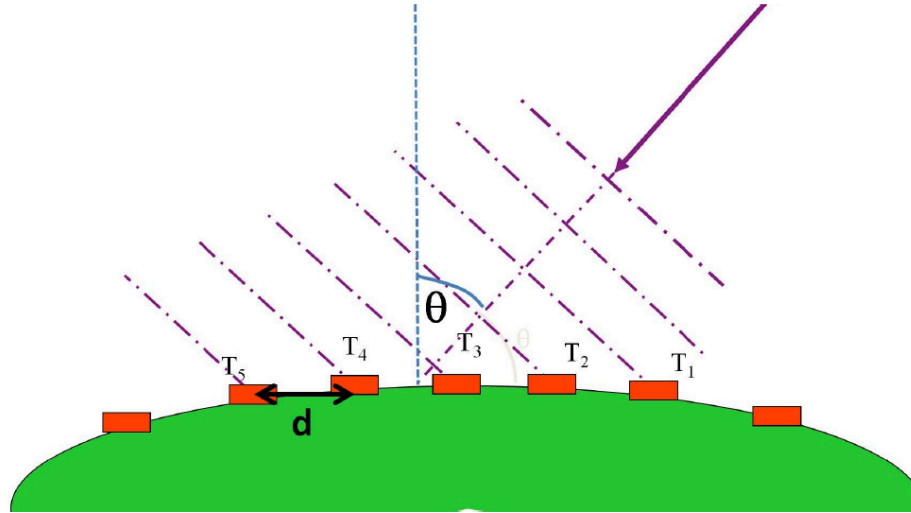
Particles traced up to 0.1 GeV

Particle showers



Muons are produced higher in the atmosphere, are more energetic and suffer less multiple scattering than electrons. Two different shower fronts build up. This effect can be used to separate the electronic and muonic content of the shower. Typical time delays in the shower core is $\sim 5\text{ns}$.

Particle showers

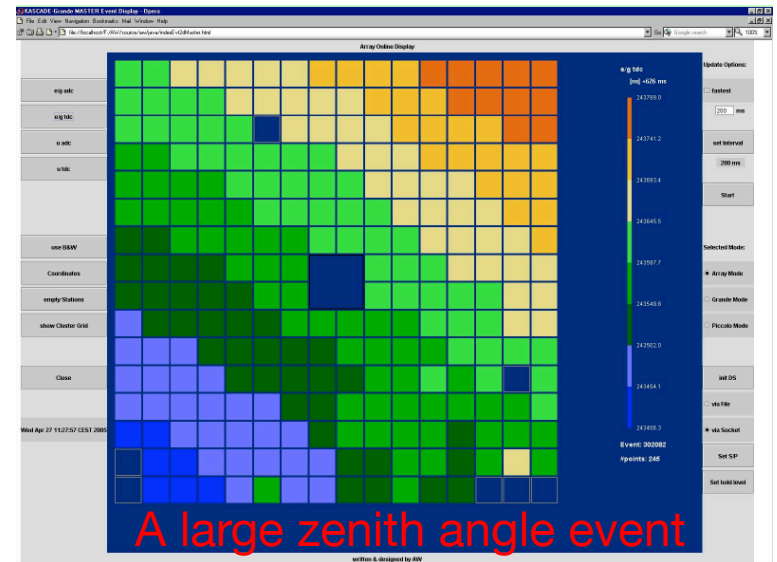
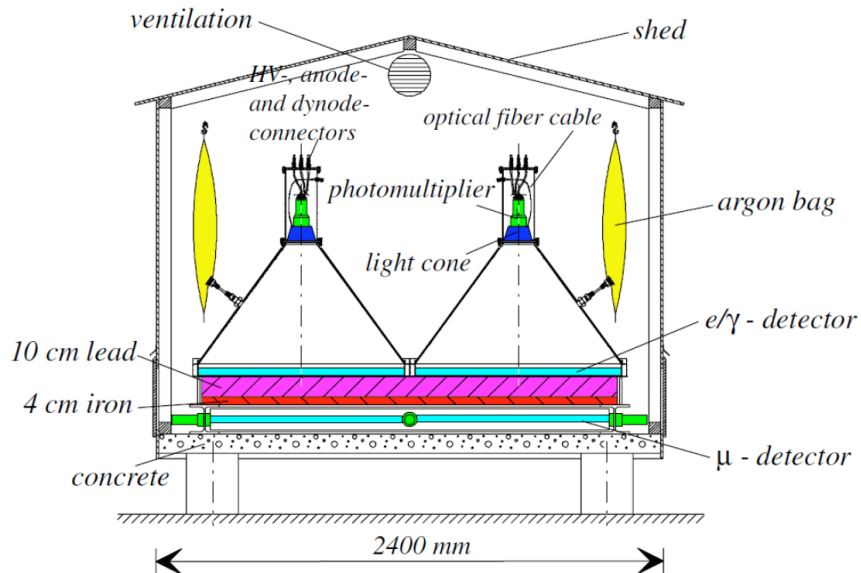


The reconstruction of the shower incoming direction is based on the different measurement times on several counters. Due to statistical fluctuations, many counters are used and the direction is estimated using best-fit techniques.

Detector Arrays

- Extensive showers are detected combining the measurements of several detector **units** spread over a **wide area** (array)
- Different detectors are used depending on the observable to be measured
- If possible, the measurement of more than one observable provides an improvement in the primary particle property accuracy
- Typical detectors used:
 - **Cherenkov tanks**
 - **Cherenkov telescopes**
 - **Fluorescence telescopes**
 - **Muon detectors**

Detector Arrays

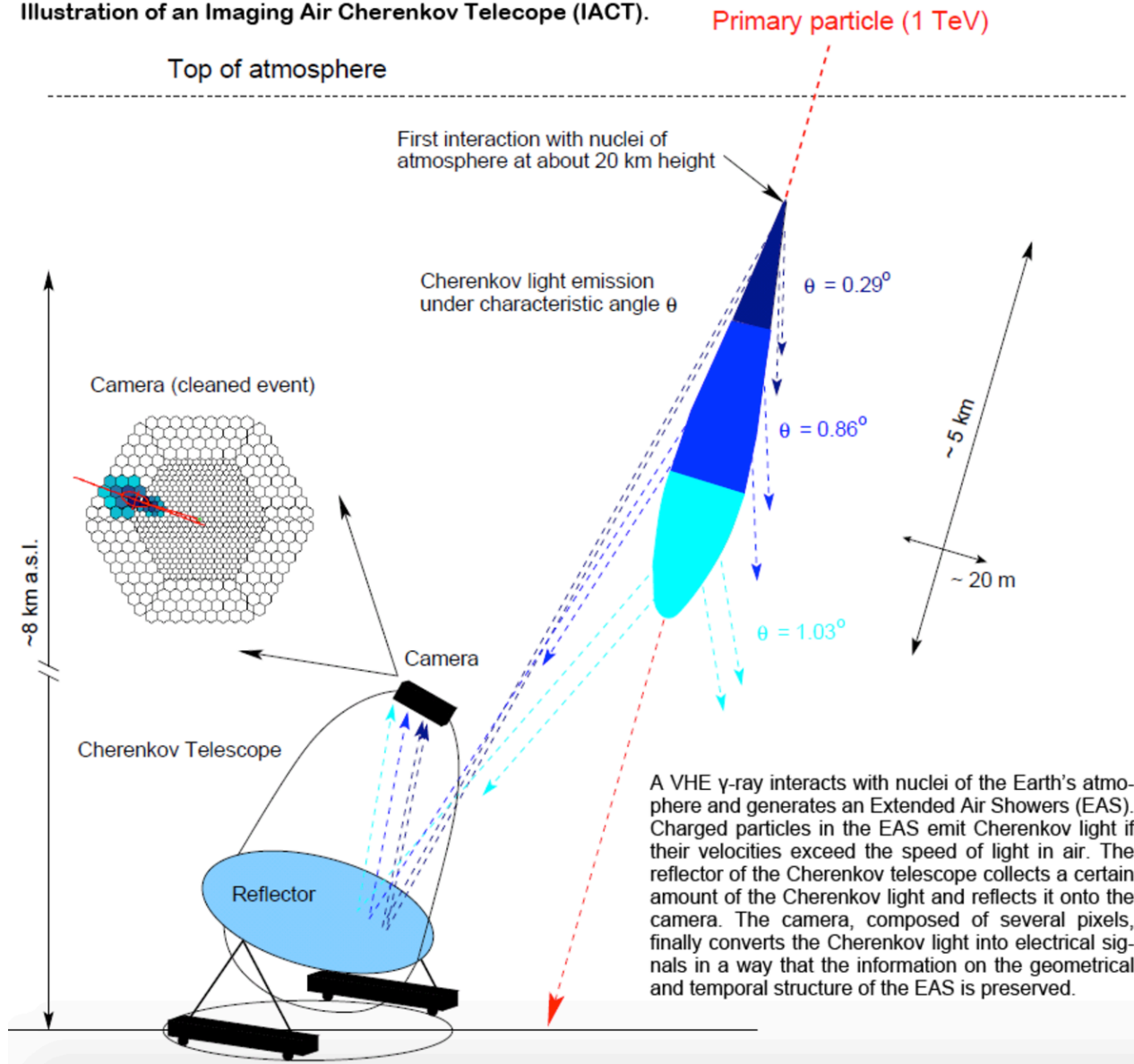


Cherenkov radiation

- In addition to the direct detection of the shower components, it is interesting to measure **indirectly** to amount of particles in the shower.
- **Cherenkov radiation**
 - **Particle travelling faster than the speed of light yield a cone of Cherenkov radiation, with a typical angular aperture of $O(1)^\circ$**
 - The light yield is emitted in a directional cone, with a yield of $O(10)$ photon/m for each shower particle above threshold. The number of emitted photon is proportional to the number of particles in the shower, therefore to the primary particle energy
 - The light cone is highly collimated and extends in an area of $O(100\text{m}^2)$ at ground
 - Photons are emitted in the UV regions → can be collected by UV-sensitive photosensors on imaging cameras

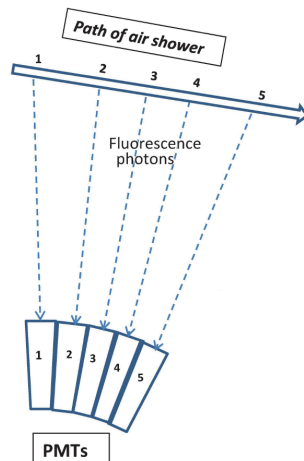
Imaging Cherenkov telescope

Illustration of an Imaging Air Cherenkov Telescope (IACT).

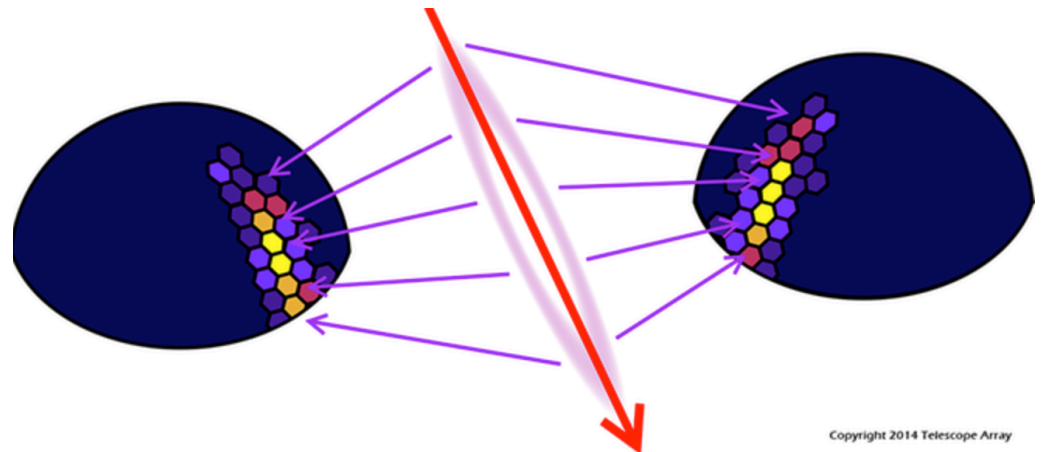


Fluorescence detector

- In addition to the direct detection of the shower components, it is interesting to measure **indirectly** to amount of particles in the shower.
- **Fluorescence radiation:**
 - High energy particles of the shower excite or ionize nitrogen molecules. N_2^* de-excites in $O(10)$ ns and emits isotropically near UV photons, with a yield of $O(5\sim 10)$ photons/m. The light yield is prop. to the number of charged particle at that height.
 - The shower profile can be observed from any direction, allowing to precisely reconstruct the shower profile development
 - Due to the small yield, only shower with $E > 10^{18}$ eV produce a measurable intensity of fluorescence light
 - Low duty cycle (only $\sim 10/15\%$, during moonless nights)

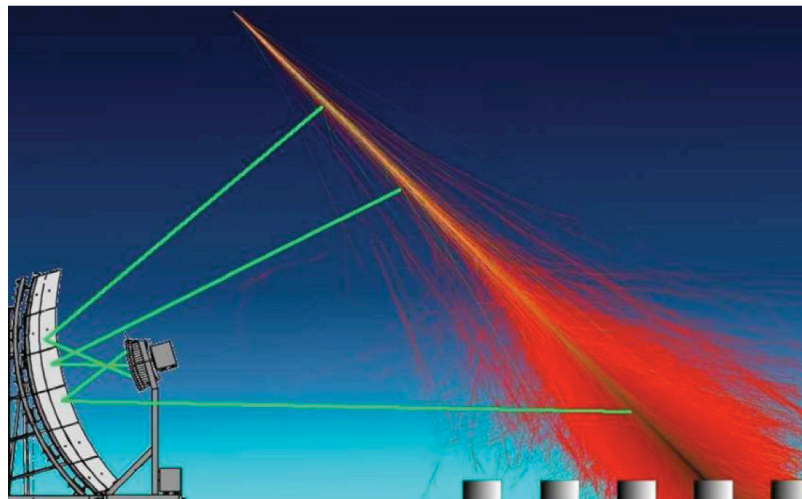


Fly's Eye technique (1981-1992)

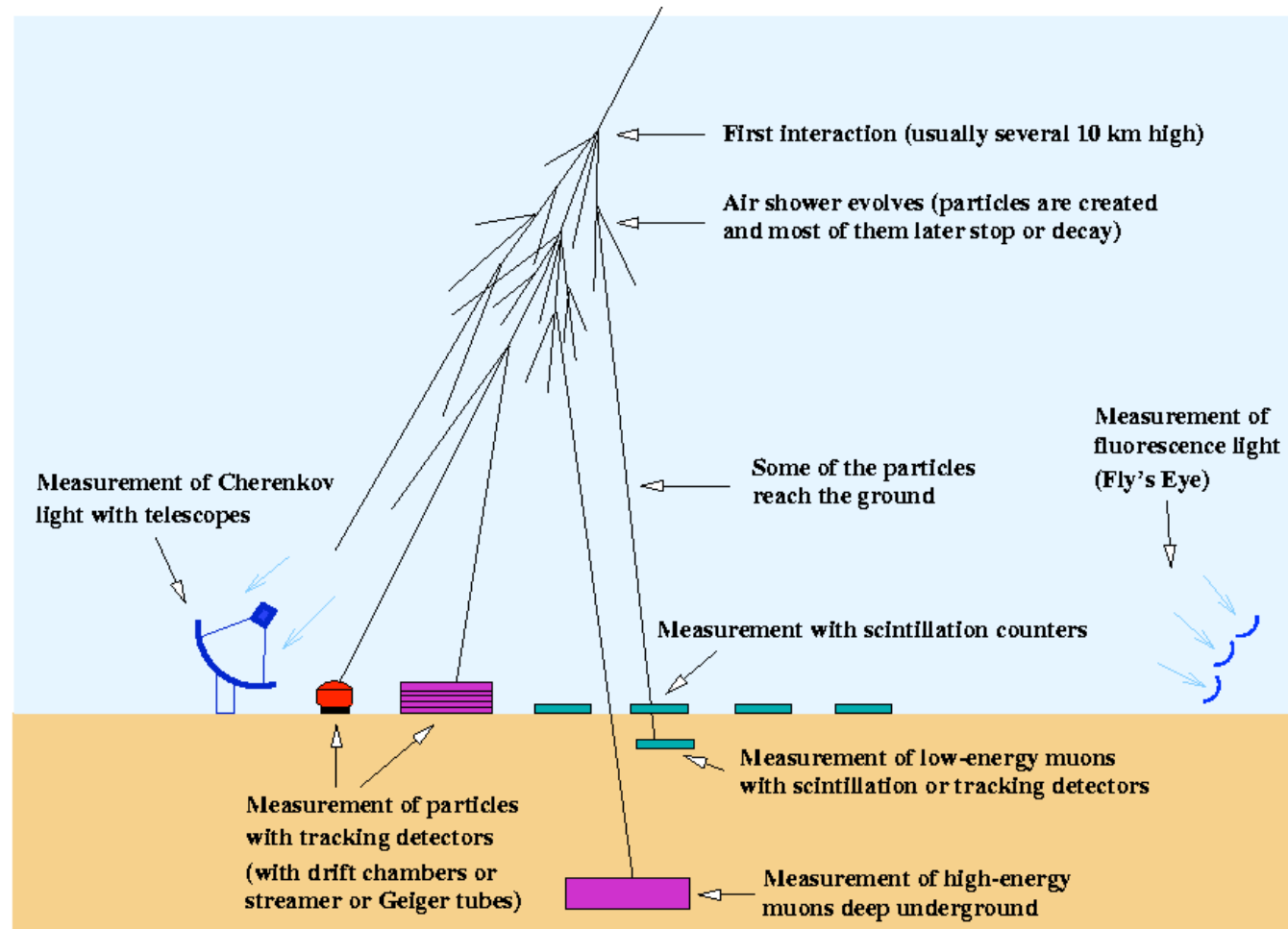


Fluorescence detector

- In addition to the direct detection of the shower components, it is interesting to measure **indirectly** to amount of particles in the shower.
- **Fluorescence radiation:**
 - High energy particles of the shower excite or ionize nitrogen molecules. N_2^* de-excites in $O(10)$ ns and emits isotropically near UV photons, with a yield of $O(5\sim 10)$ photons/m. The light yield is prop. to the number of charged particle at that height.
 - The shower profile can be observed from any direction, allowing to precisely reconstruct the shower profile development
 - Due to the small yield, only shower with $E > 10^{18}$ eV produce a measurable intensity of fluorescence light
 - Low duty cycle (only $\sim 10/15\%$, during moonless nights)



Hybrid detectors

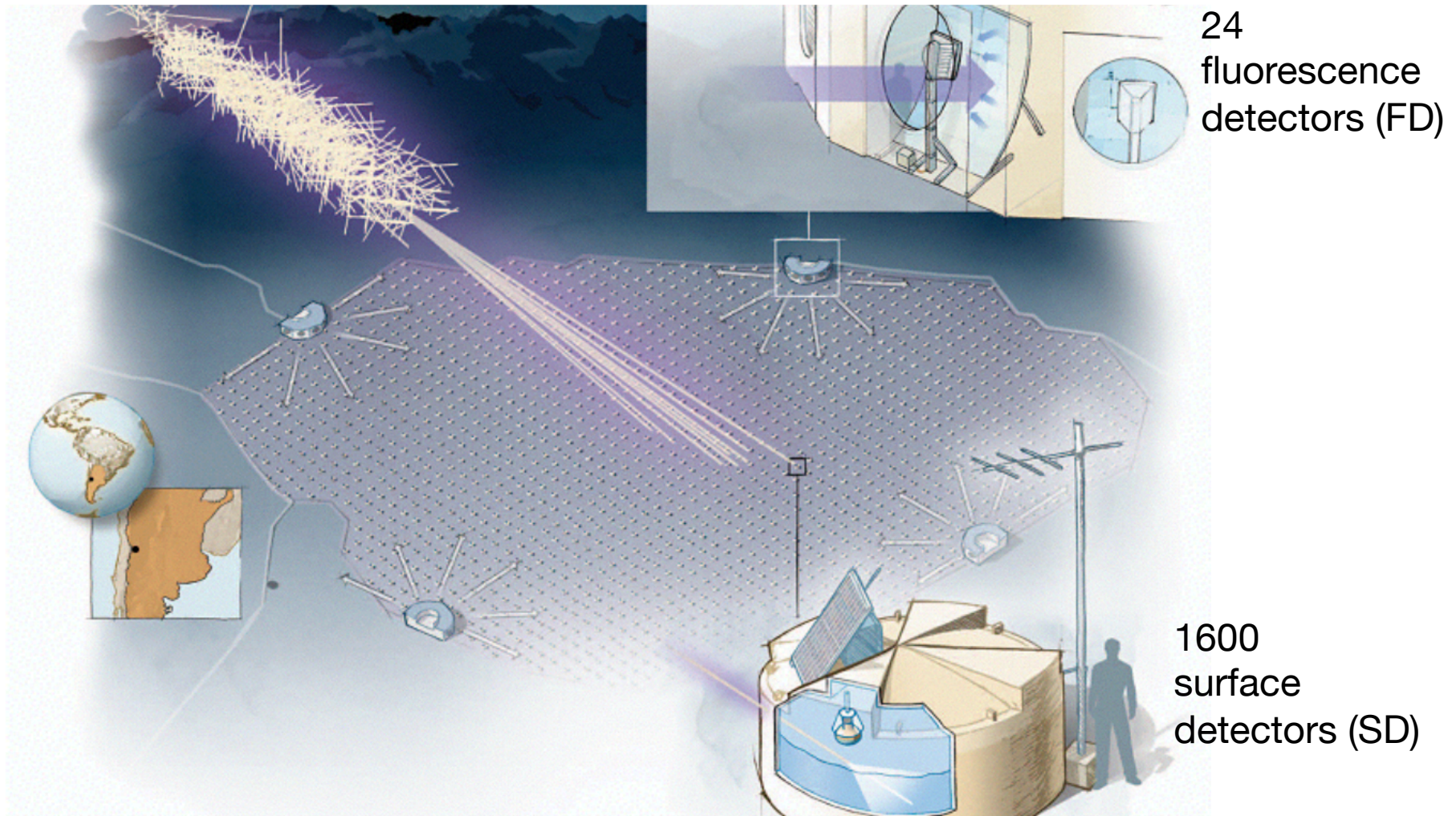


(C) 1999 K. Bernlöhr

The primary cosmic ray properties are measured by **higher sensitivities when the shower properties are measured by means of several techniques**

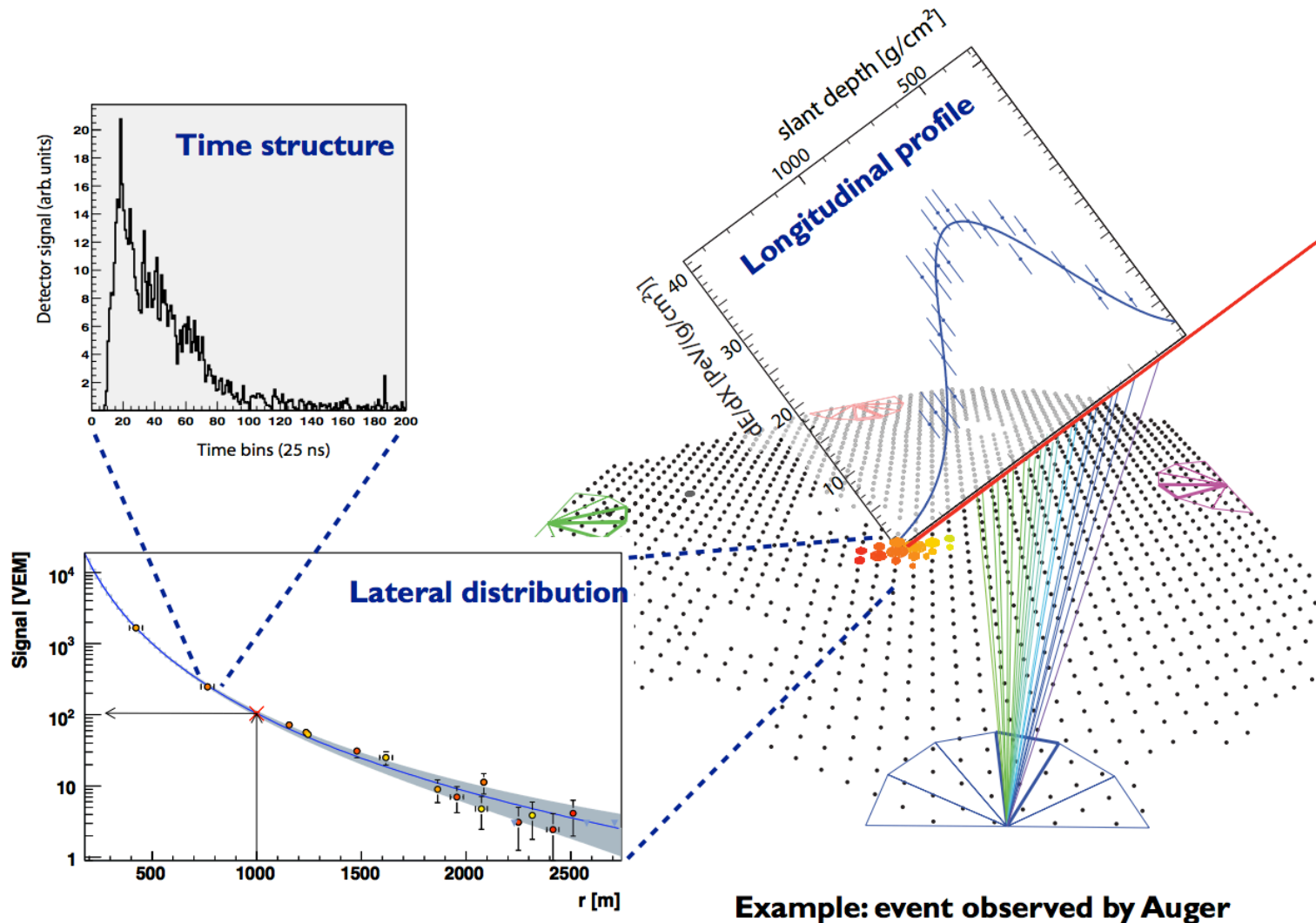
Pierre Auger Observatory

The state-of-the-art extensive air shower detector is the Pierre Auger observatory



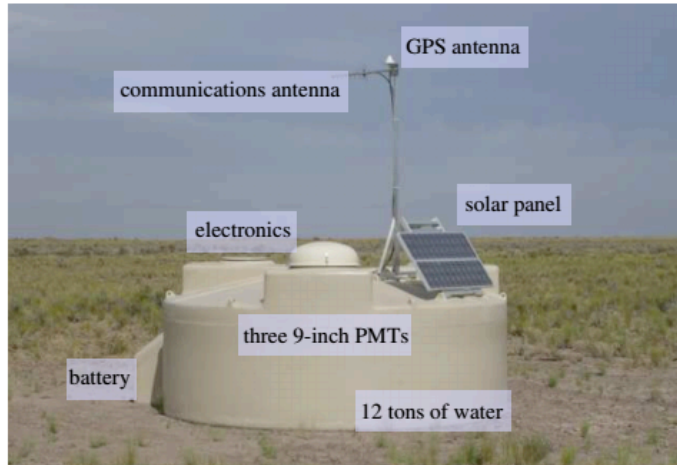
Pierre Auger Observatory

Several shower observables

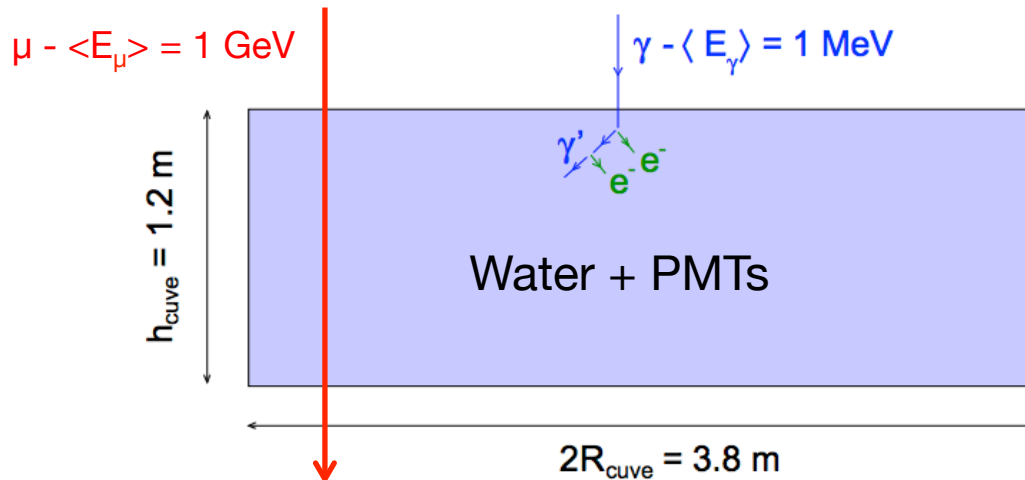


Pierre Auger Observatory

The Surface Detector / SD



- 100% duty cycle
- full acceptance for $E \geq 3 \times 10^{18} \text{ eV}$

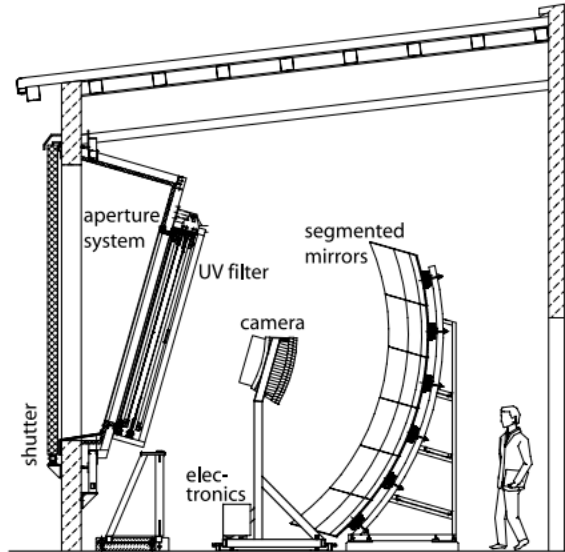


Muons at ground release much higher Cherenkov radiation than the EM component

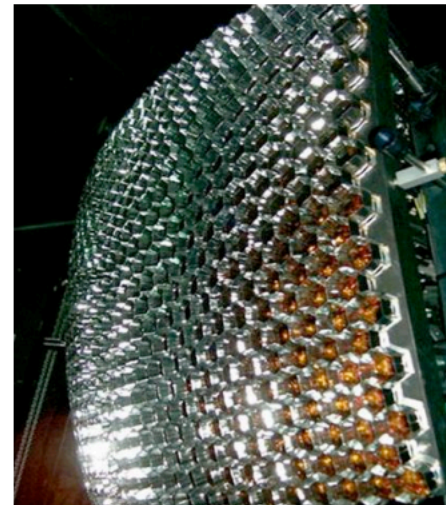
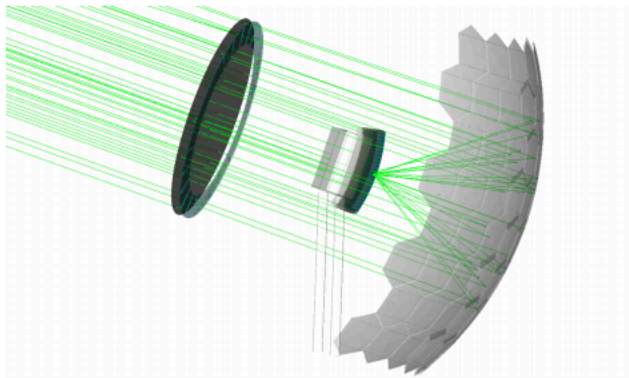
Energy deposit expressed in Equivalent Vertical Muon
 $EVM = 240 \text{ MeV}$

Pierre Auger Observatory

The Fluorescence Detector / FD



- 6 mirrors per building,
- each $30^\circ \times 30^\circ$ field of view,
- 440 PMT pixels per camera,
- UV filter.



Pierre Auger Observatory

Atmospheric Monitoring and Calibration

Atmospheric Monitoring



Central Laser Facility

Absolute Calibration



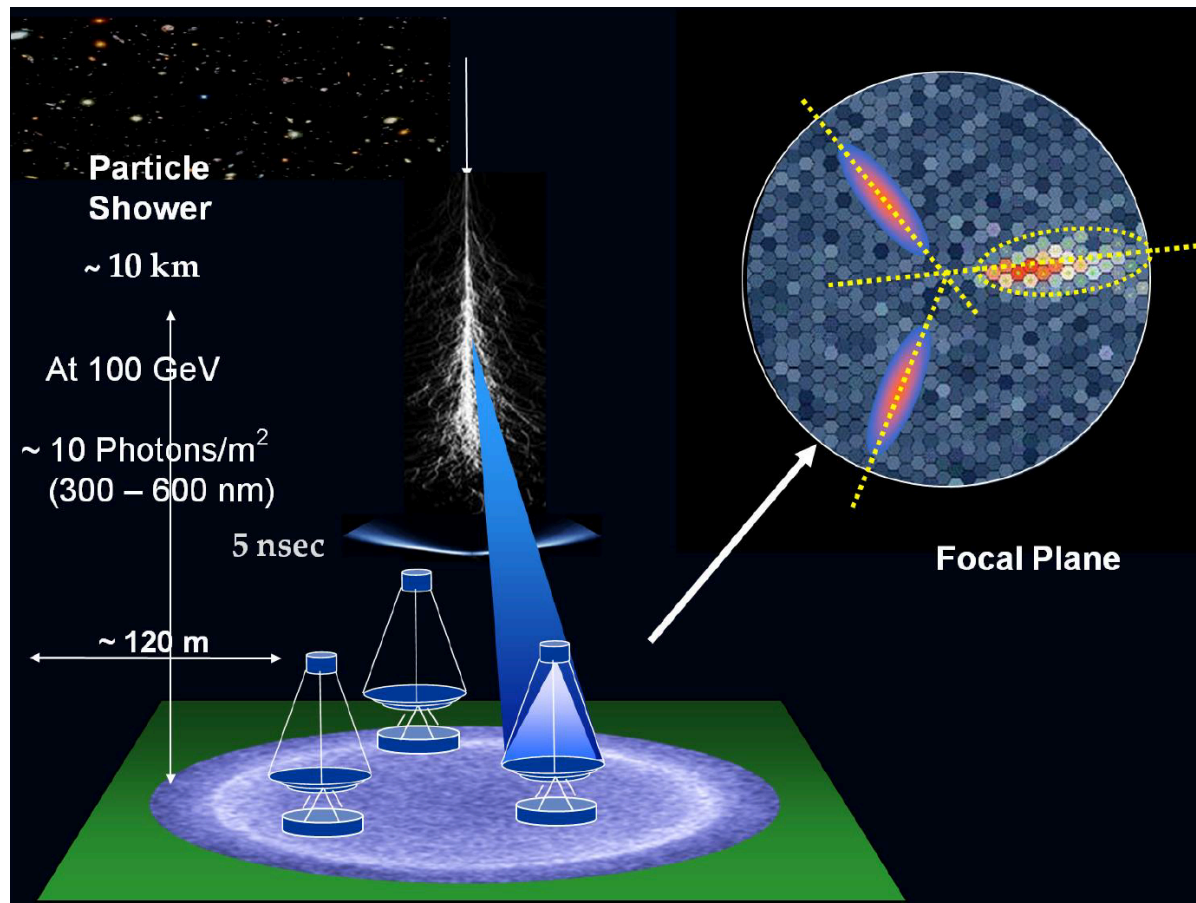
Drum for uniform illumination of the camera used for calibration.



LIDAR in each fluorescence detector building

Imaging Air Cherenkov Telescopes

- Imaging Air Cherenkov Telescopes (IACTs) are primarily used to **detect electromagnetic cascades initiated by high energy gamma-rays and e^{\pm}**
- Imaging: the Cherenkov light is focused in a multi-pixel camera to reconstruct the shower properties



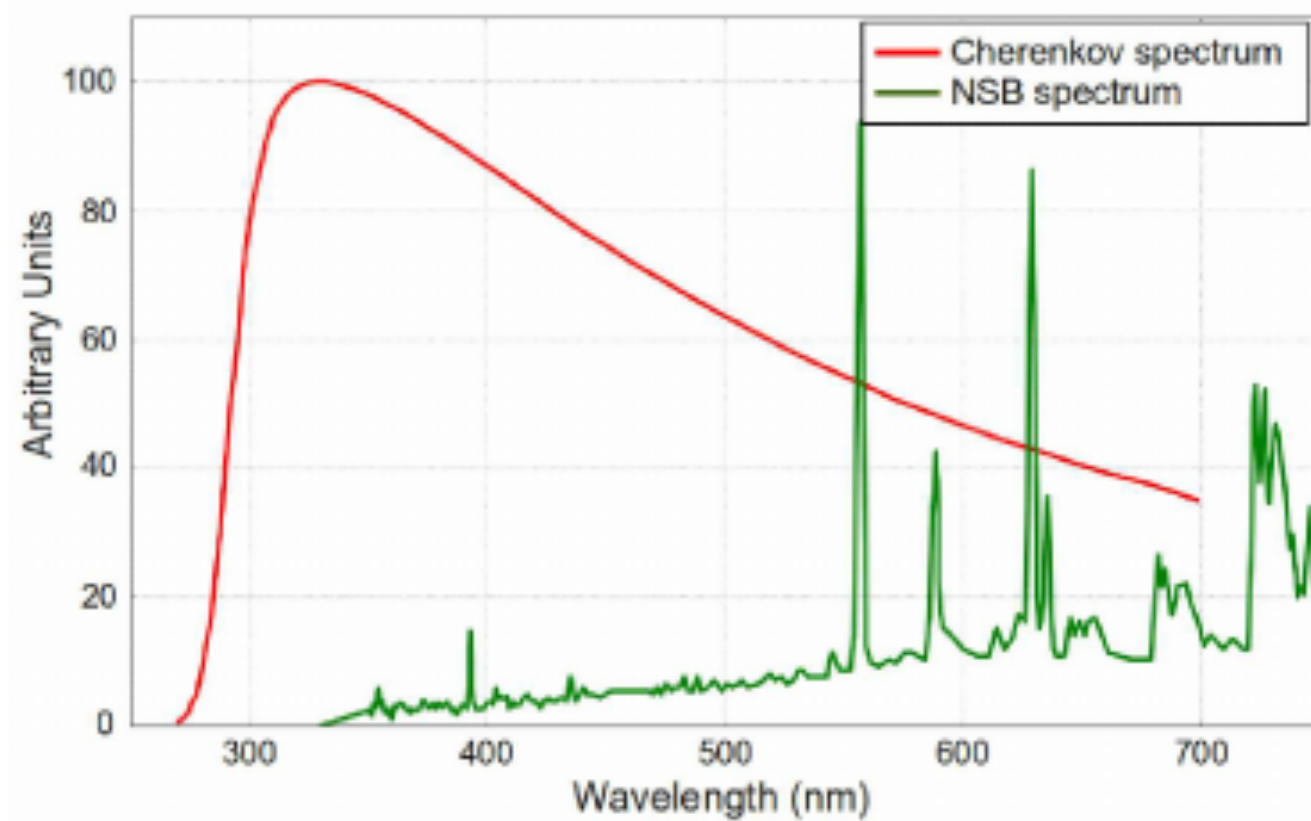
Imaging Air Cherenkov Telescopes

NIGHT SKY BACKGROUND

- Moon
- Airglow
 - the brightest component and is caused by oxygen atoms glowing in the upper atmosphere which are excited by solar ultraviolet radiation. Airglow gets worse at solar maximum. (increases towards red)
- Zodiacal light
 - Interplanetary dust particles reflect and scatter sunlight and make up the zodiacal light and gegenschein (increases towards red)
- Star light
 - Stars mostly from Milky way
 - includes starlight is scattered by the atmosphere, just as sunlight is during the daytime. (Slightly blue)
- Aurorae borealis:
 - Cosmic ray particles from solar wind cause glow in upper atmosphere; mostly in polar regions where they spiral down the magnetic poles.
- Moonless night sky total background: $\approx 10^{12}$ photons/(m²s sr) (\pm factor ≈ 2)

Imaging Air Cherenkov Telescopes

NIGHT SKY BACKGROUND



Imaging Air Cherenkov Telescopes

- Night sky background: $\Phi_{NSB} = 10^{12}$ photons/(m² s sr)
- Cherenkov pulse: $\Phi_{Ch} = 10$ photons/m²/3ns
- Transmittance of atmosphere
- qE =quantum efficiency
- Instruments: PMT, mirrors, electronics
- Number of signal photoelectrons: $\Phi_{Ch} \cdot A \cdot T \cdot qE$
- Number of background photoelectrons: $\Phi_{NSB} \cdot A \cdot T \cdot qE \cdot \tau \cdot \Omega$
- Solid angle greater than shower (> 1 degree)

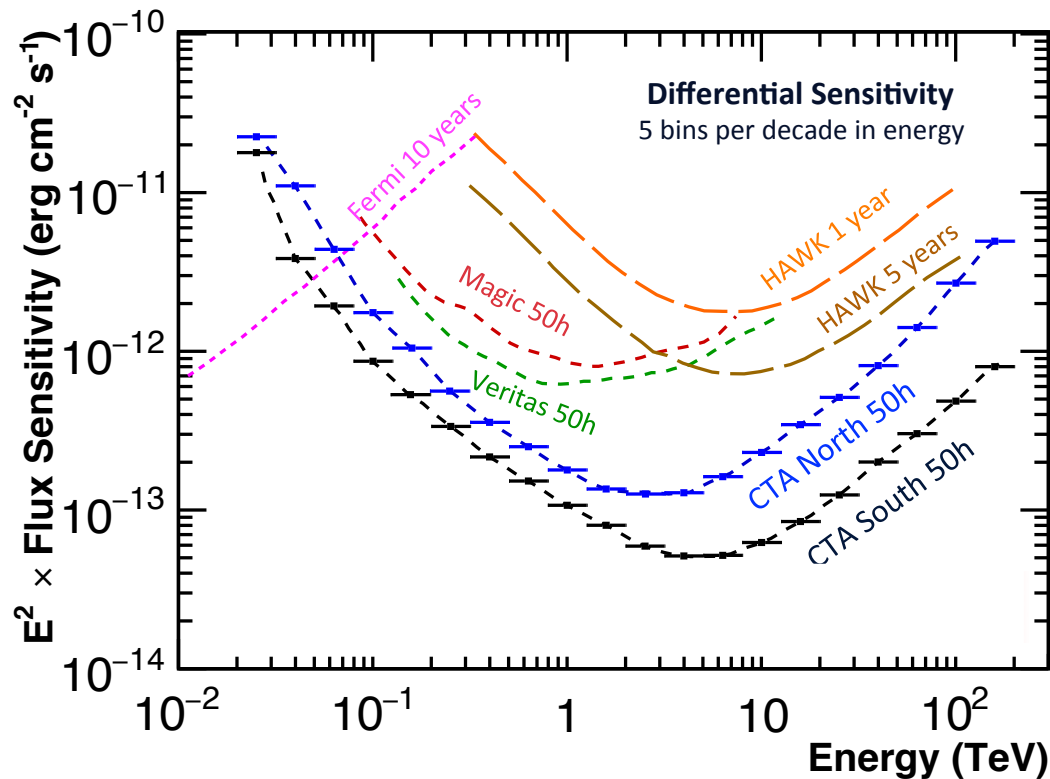
$$\frac{Signal}{Noise} = N_{\sigma} = \frac{\Phi_{ch} \cdot A \cdot T \cdot qE}{\sqrt{\Phi_{NSB} \cdot A \cdot \Omega \cdot T \cdot qE \cdot \tau}}$$

$$N_{\sigma} = \Phi_{ch} \sqrt{\frac{T \cdot A \cdot qE}{\Phi_{NSB} \cdot \Omega \cdot \tau}}$$

To achieve a reasonable S/N, detector, we have to tune A and Ω .
The solution involves the pixelation of the camera (small Ω per channel), with the possibility to trigger the event only if an interesting pattern of fired pixel is measured in the camera

Imaging Air Cherenkov Telescopes

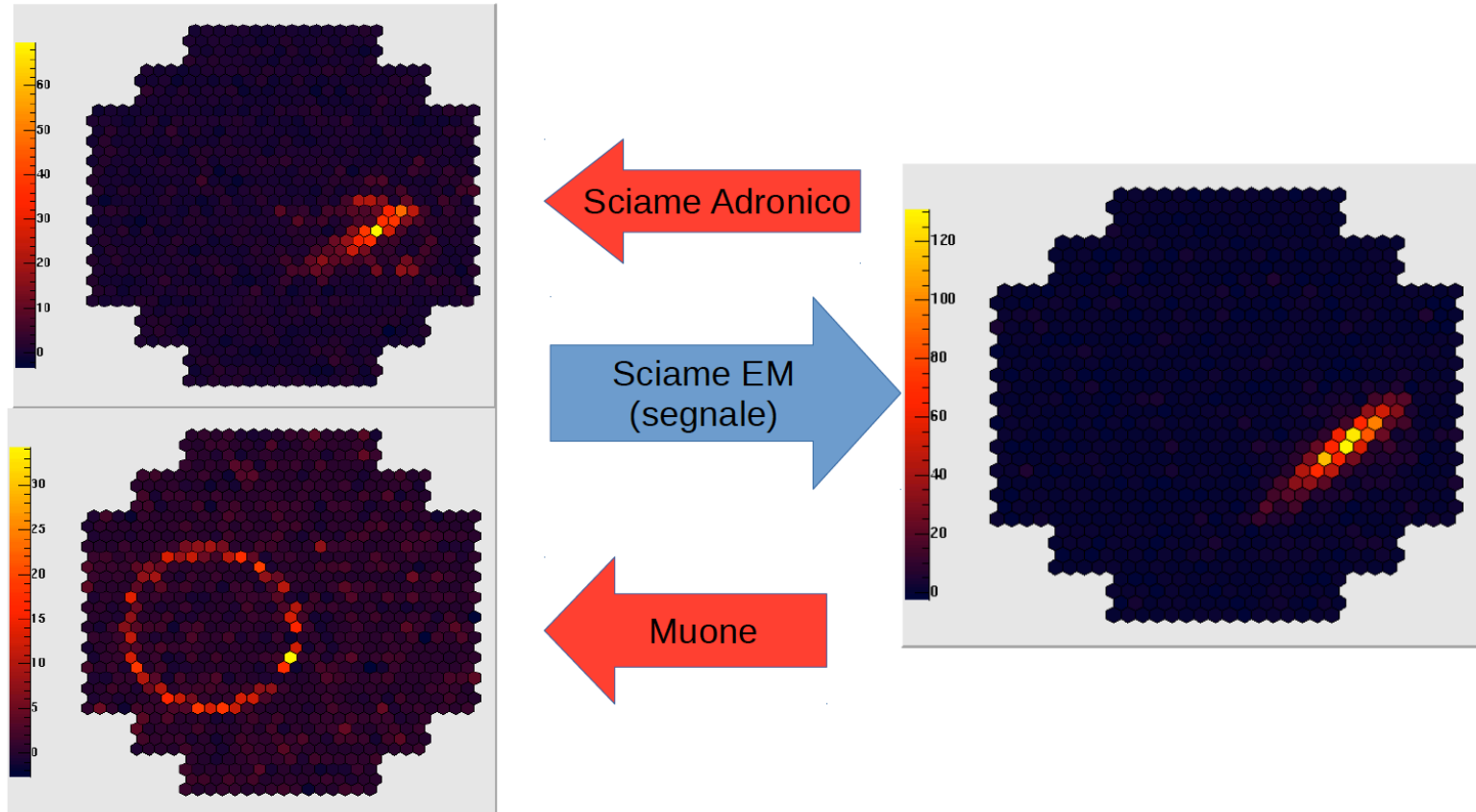
- IACTs provide improved sensitivity in the high energy range, where the sensitivity of space borne detectors is limited by their low acceptance



Imaging Air Cherenkov Telescopes

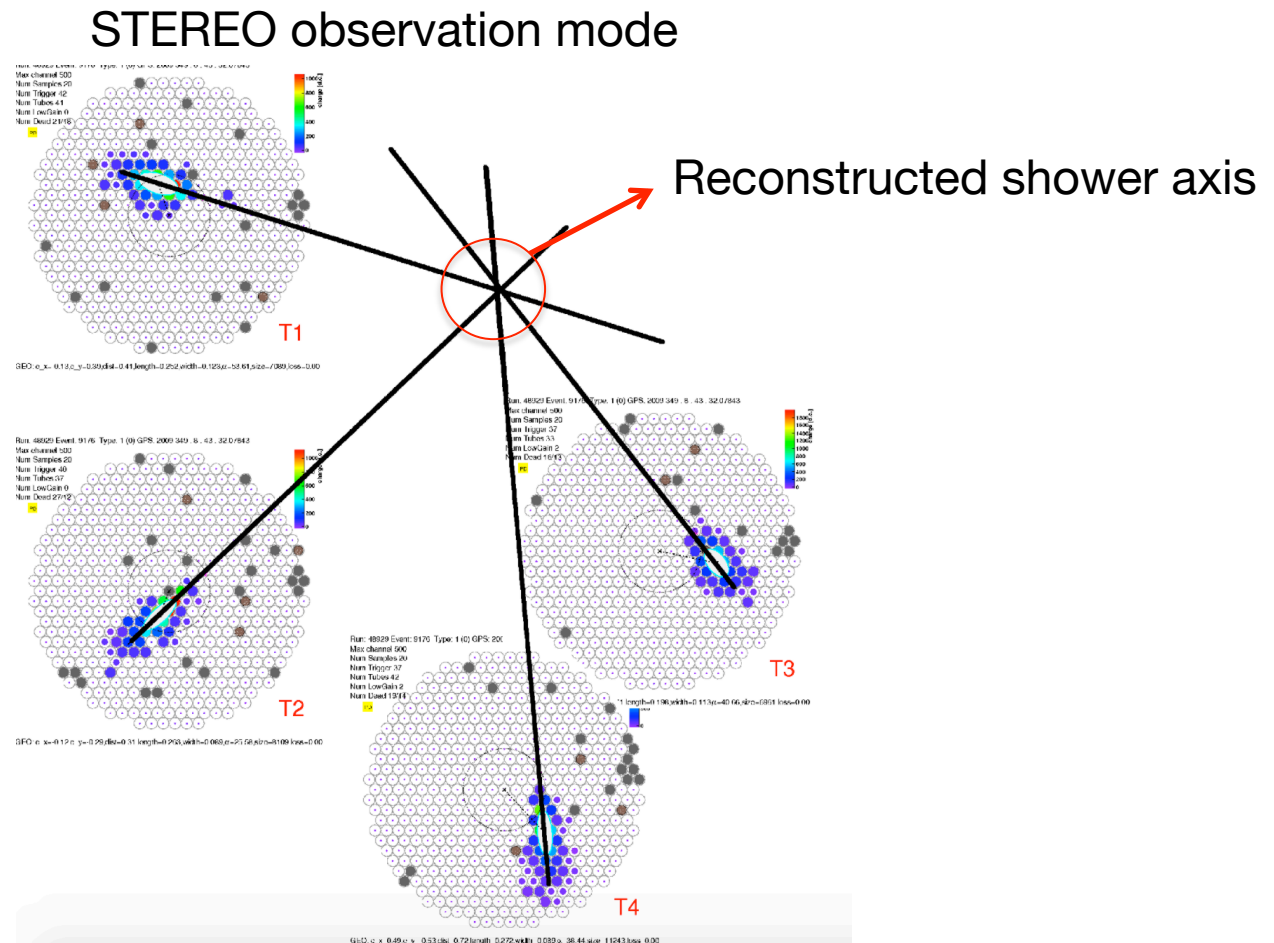
- Imaging reconstruction allows to separate the interesting EM signal from the background hadronic shower or muon rings

MONO observation mode



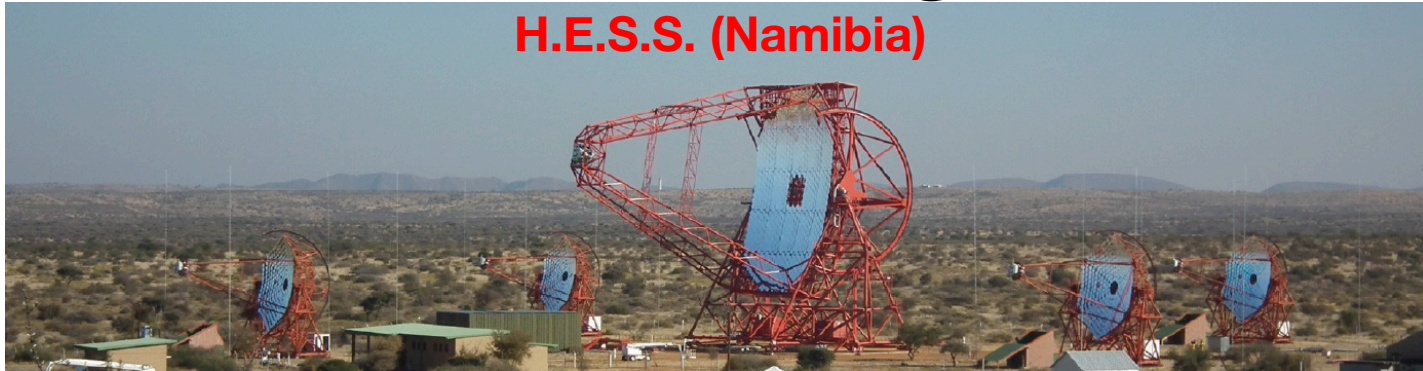
Imaging Air Cherenkov Telescopes

- Imaging reconstruction allows to separate the interesting EM signal from the background hadronic shower or muon rings



The current IACT generation

H.E.S.S. (Namibia)



VERITAS (Arizona)



MAGIC (La Palma)

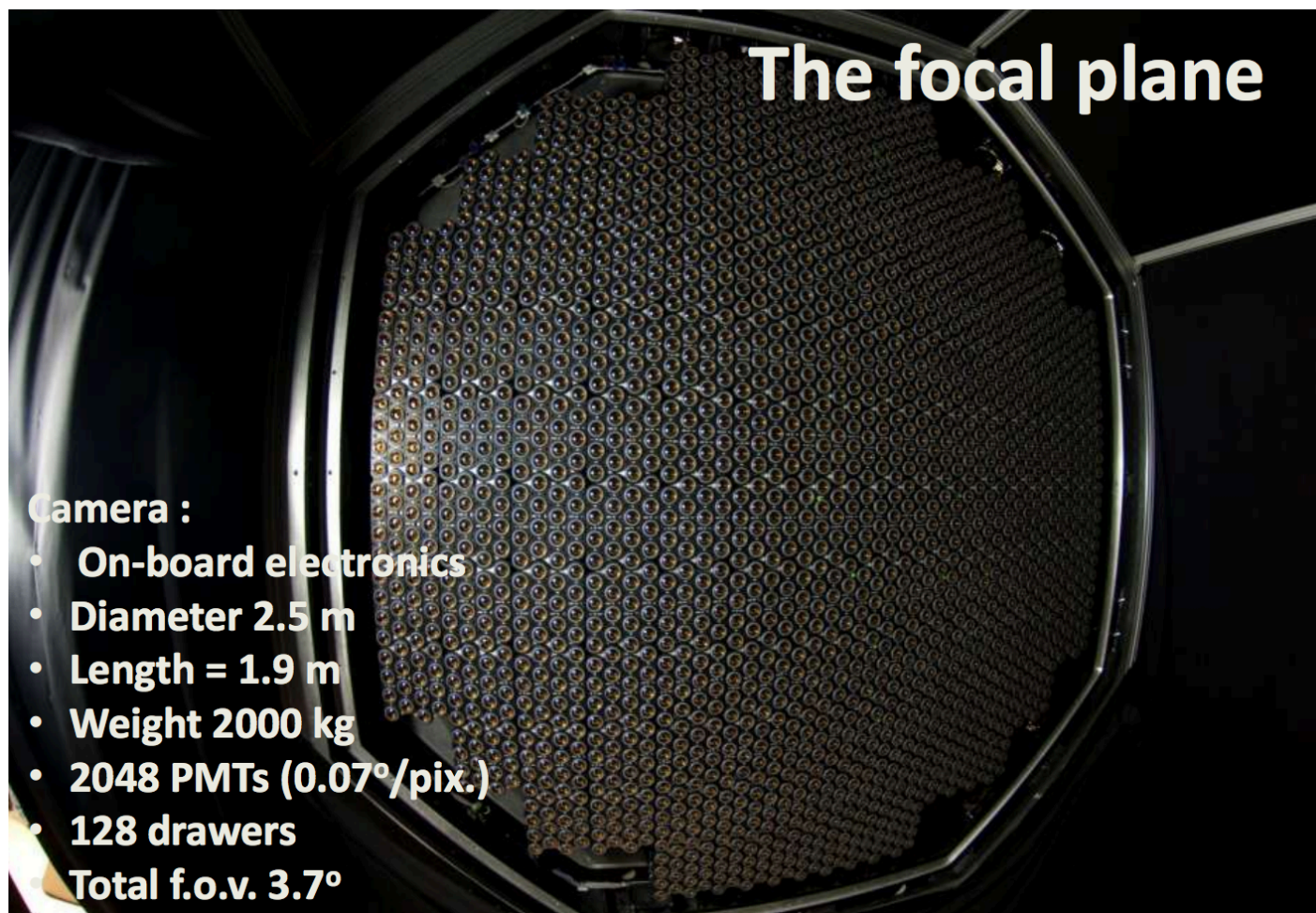


Performances:

- Sensitive to primary photons in the 100 GeV – 10 TeV energy range
- Energy resolution $\sim 20\%$
- Duty cycles $< 15\%$
- Angular resolution $\sim 0.1^\circ$ at high energies

The Cameras

The HESS II camera



Camera :

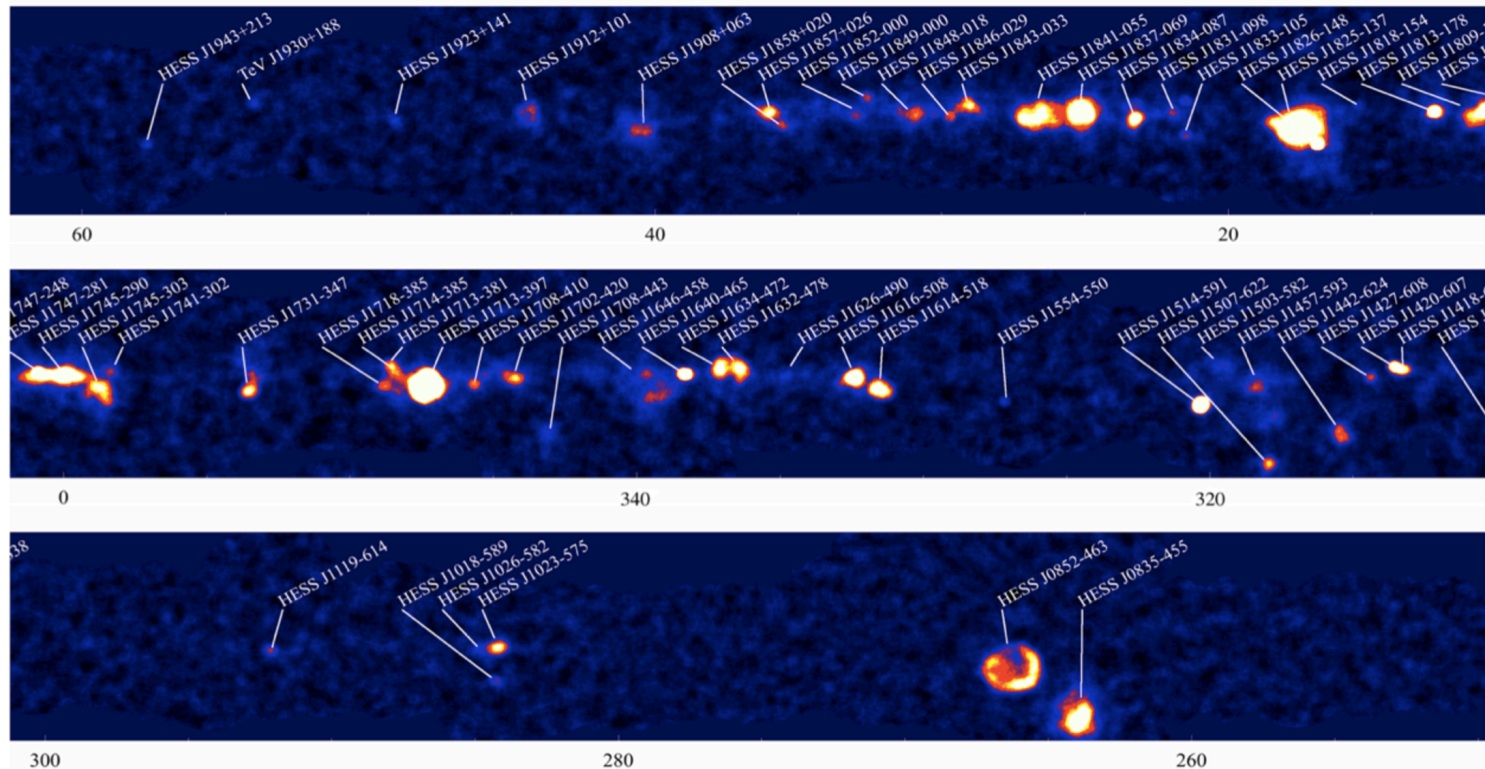
- On-board electronics
- Diameter 2.5 m
- Length = 1.9 m
- Weight 2000 kg
- 2048 PMTs (0.07°/pix.)
- 128 drawers
- Total f.o.v. 3.7°

PMTs with a maximum Photon Detection Efficiency of 30%

High energy gamma-ray science

- The science targeted by IACTs is very variegate, and it involves many topics of astrophysics and particle physics
- I will mention few, which are more “particle-physics” related
- The field is wide, you can look up yourself if you are interested in the topics that I will not cover

HESS galactic sky survey



High energy gamma-ray science

Cosmic Ray Acceleration Mechanisms

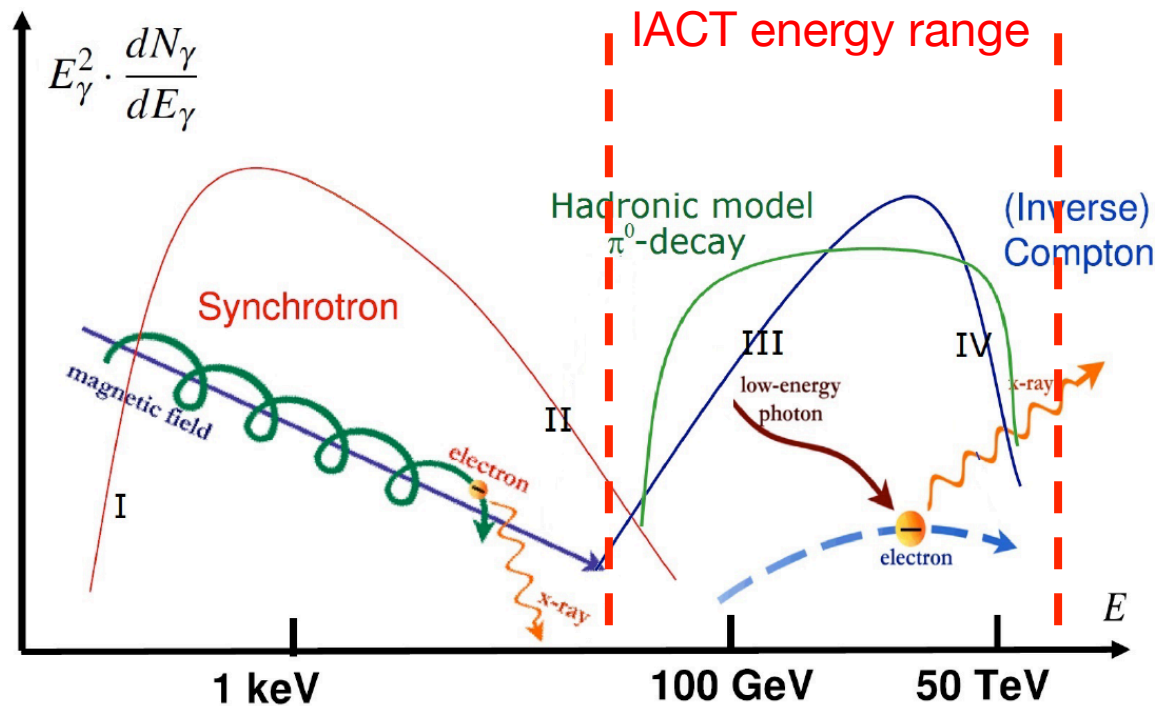


Fig. 8.1. Spectral energy distribution of photons produced in leptonic/hadronic models. Synchrotron radiation is caused by relativistic electrons accelerated in a magnetic field. Photons from synchrotron emission represent also the target for inverse Compton scattering of the parent electrons. When hadrons interact with matter or ambient photons, a distribution of γ -rays from π^0 decays as indicated by the green curve could be obtained. Superimposition of γ -rays from both leptonic and hadronic mechanisms is assumed in case of mixed models. Adapted

High energy gamma-ray science

Spectral and morphological studies of CR sources

γ -ray spectrum of RX J1713.7-3946 compared with expectations for lepton CR origin models. The same spectrum cannot however rule out the hadronic hypothesis in presence of a hard injection spectrum

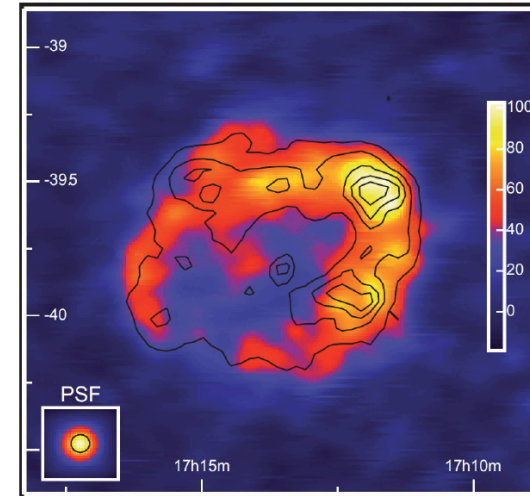
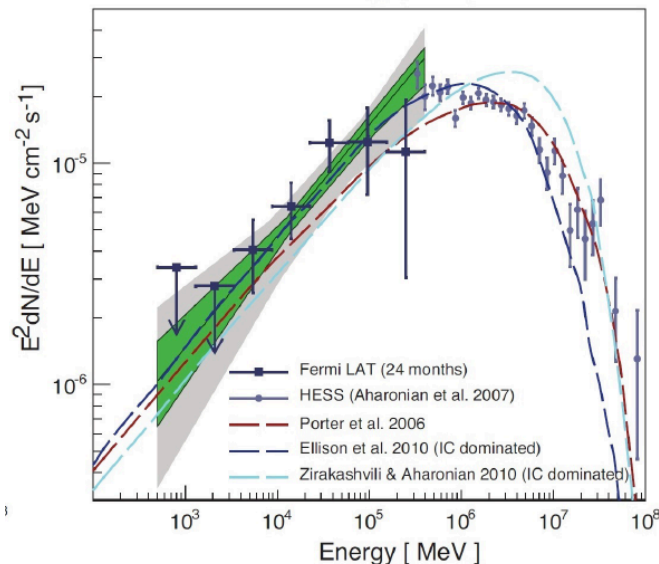


Fig. 9.11. HESS map of γ -ray excess events for RX J1713.7-3946 - the first SNR shell to be resolved at TeV energies. The superimposed contours show the X-ray surface brightness as seen by [ASCA](#) in the 1-3 keV range. On the bottom left, the HESS point spread function

The detailed morphological studies possible with IACTs at the level of 0.1° shows that the acceleration sites are spatially coincident with the sites of non-thermal X-ray emission, strengthening the hypothesis that primary galactic CRs up to the “knee” are accelerated in SNRs. The identification of these objects is still an open field

High energy gamma-ray science

Dark Matter indirect searches

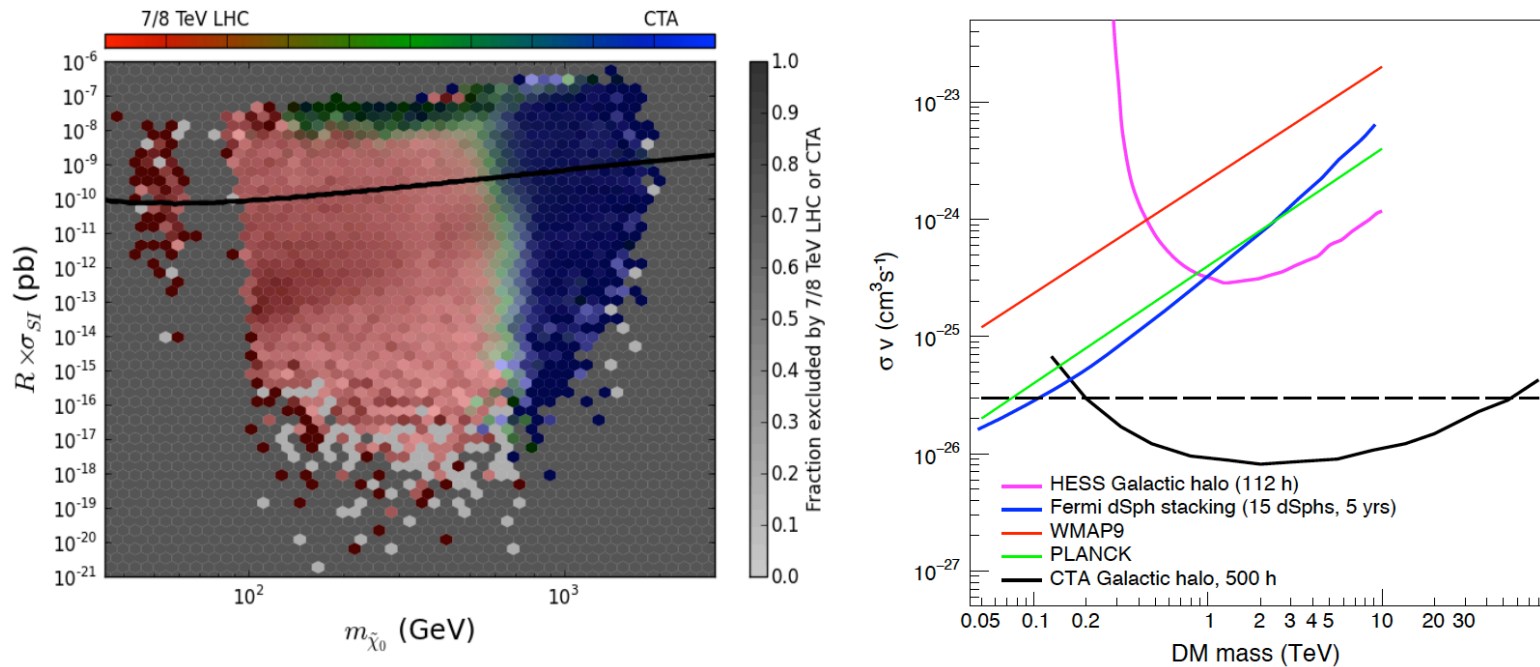
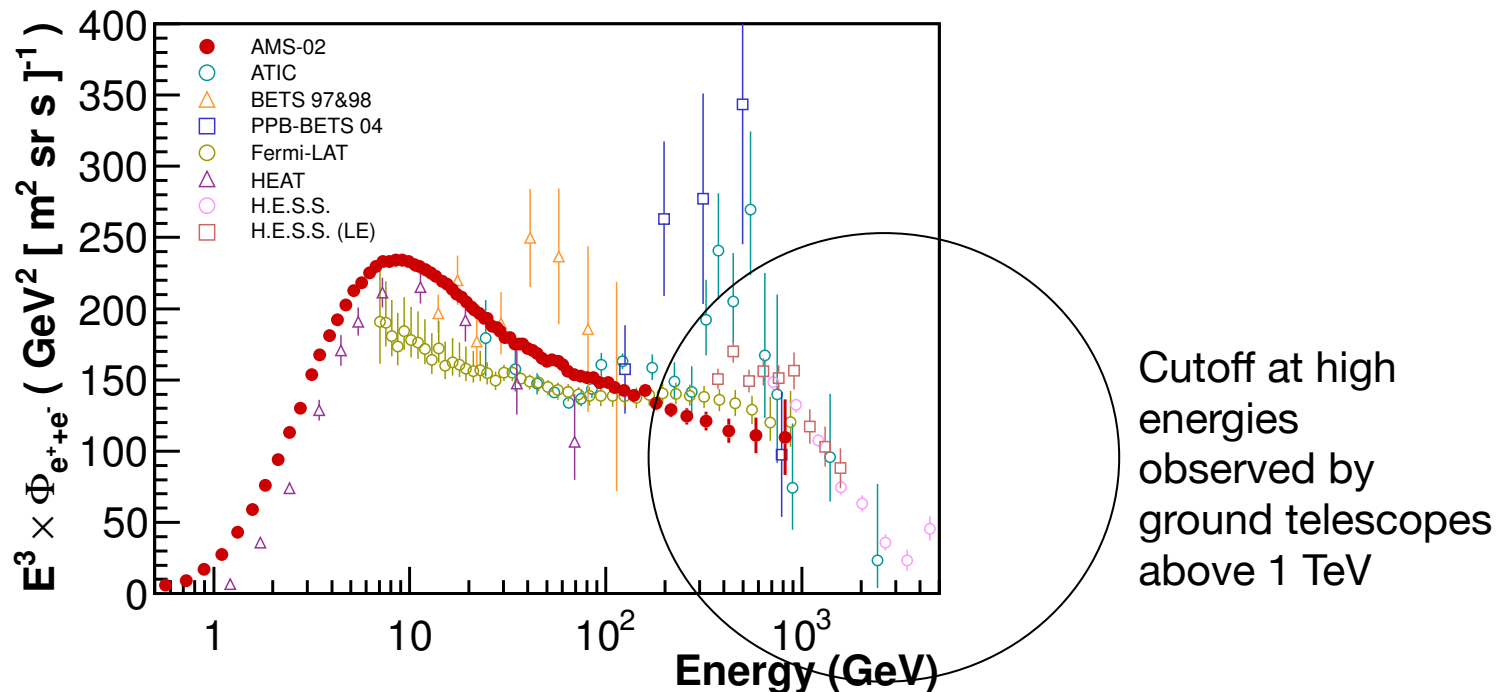


Figure 4.3 – Left: Comparisons of models from the phenomenological minimal supersymmetric model (pMSSM) surviving or being excluded by future direct-detection, indirect-detection and collider searches in the neutralino mass-scaled spin-independent cross section plane. The spin-independent XENON1T exclusion is shown as a solid black line. Figure extracted from [74]. Left: Current best limits on the annihilation cross section from indirect detection (Fermi-LAT and H.E.S.S.) and cosmic microwave background (WMAP and Planck) experiments [52]. Also shown is the projected sensitivity for CTA from observations of the Galactic halo.

High energy gamma-ray science

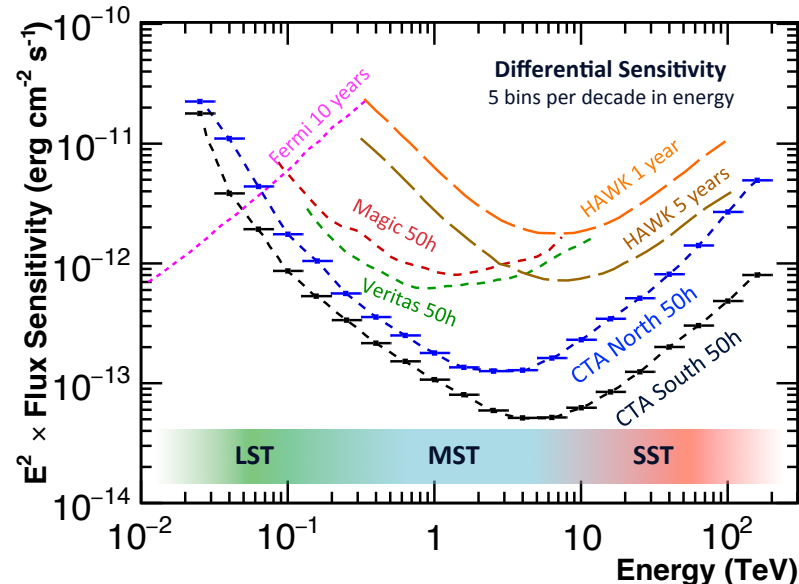
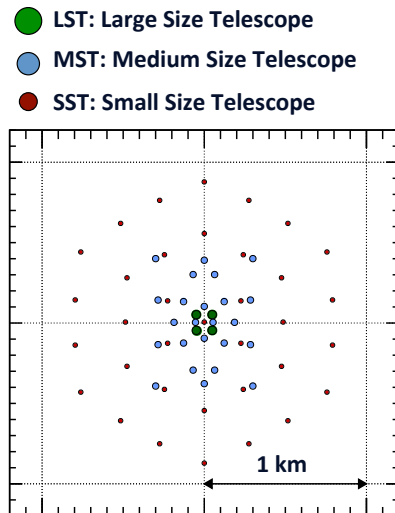
Electron + Positron spectrum

- IACTs cannot distinguish between photon-initiated showers and electron/positron initiated showers
- e^{\pm} are identified as EM showers when pointing out of gamma-ray sources (photons keep directionality, e^{\pm} are \sim isotropic)
- Complementarity with space born experiments: extension of spectra at higher energies (but worst accuracy due to energy scale uncertainty and hadronic and gamma-ray background)



The next IACT generation

- **The Cherenkov Telescope Array** is a project that intends to improve the current IACT telescope sensitivities and extend the maximum energy range up to 100 TeV photons.
- To achieve this target, the community efforts are focused towards a unique, global project that intends to build two arrays of telescopes, one in the northern hemisphere and one in the southern hemisphere, to achieve a complete coverage of the sky.



Two sites (North and South) for a whole-sky coverage

Operated as an open Observatory

A factor of 5-20 more sensitive w.r.t. the current IACTs depending on the energy band

A few large size telescopes to cover the range 20 - 150 GeV

~km² array of medium size telescopes for the 0.15 - 5 TeV domain

~4km² array of small size telescopes, sensitive above 5 TeV up to 300 TeV

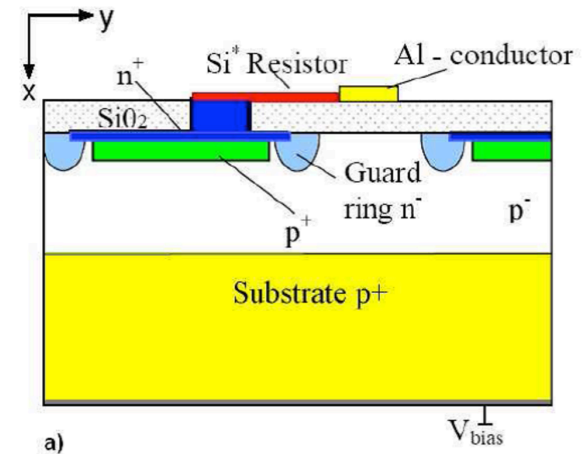
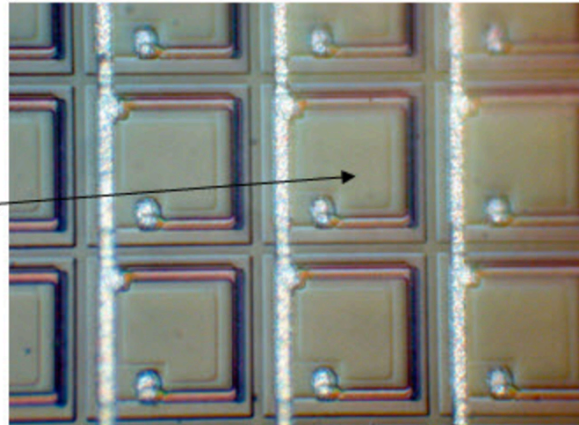
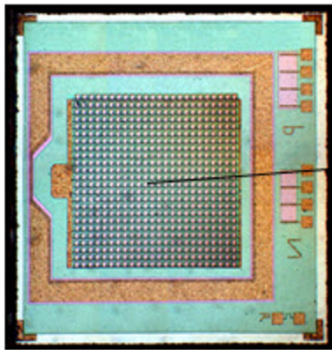
4 LSTs [N & S]

15 MSTs [N]
25 MSTs [S]
(24 SCTs [S])

70 SSTs [S]

CTA SiPM Camera

- Many CTA camera will be equipped **using Silicon Photomultipliers instead of PMTs**
 - Better sensitivity, more robust, can be operated with less than 100V



SiPM: array of microcell APD operated in geiger mode. For low light intensity, the number of fired cells is proportional to the number of photons

CTA SiPM Camera

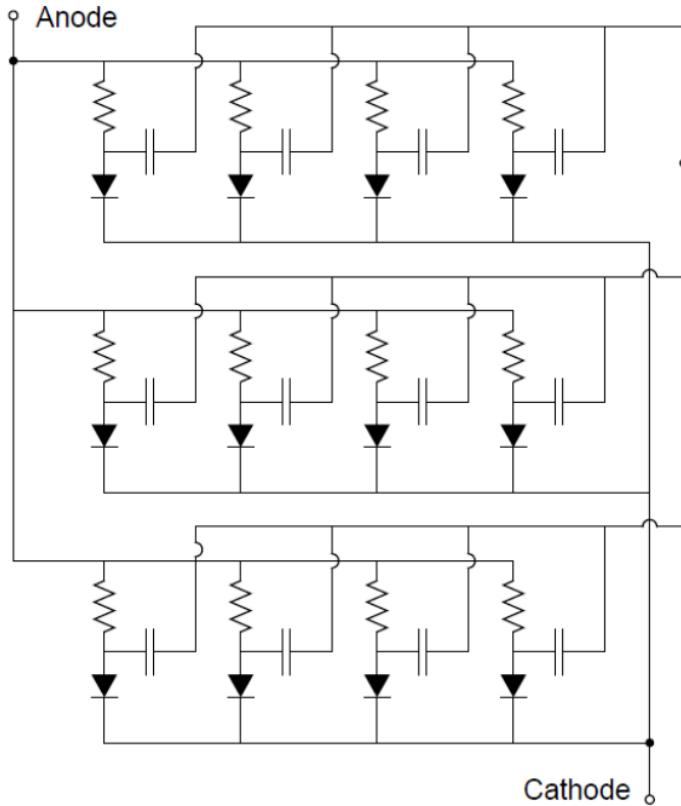


Figure 4, An SiPM consists of an array of microcells (photodiode plus quench resistor) with summed output. The fast output is discussed in section 1.5.

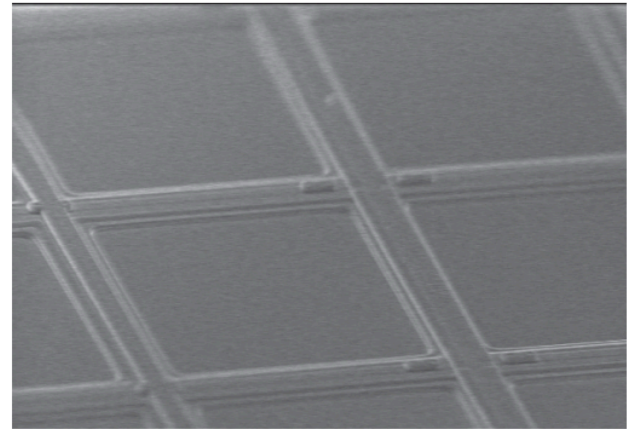


Figure 5, Image showing the microcell structure of the SiPM surface

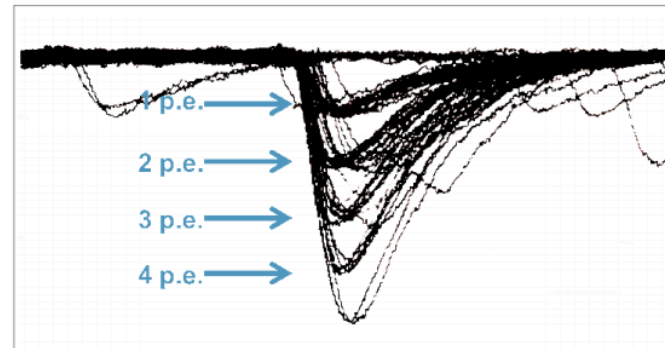
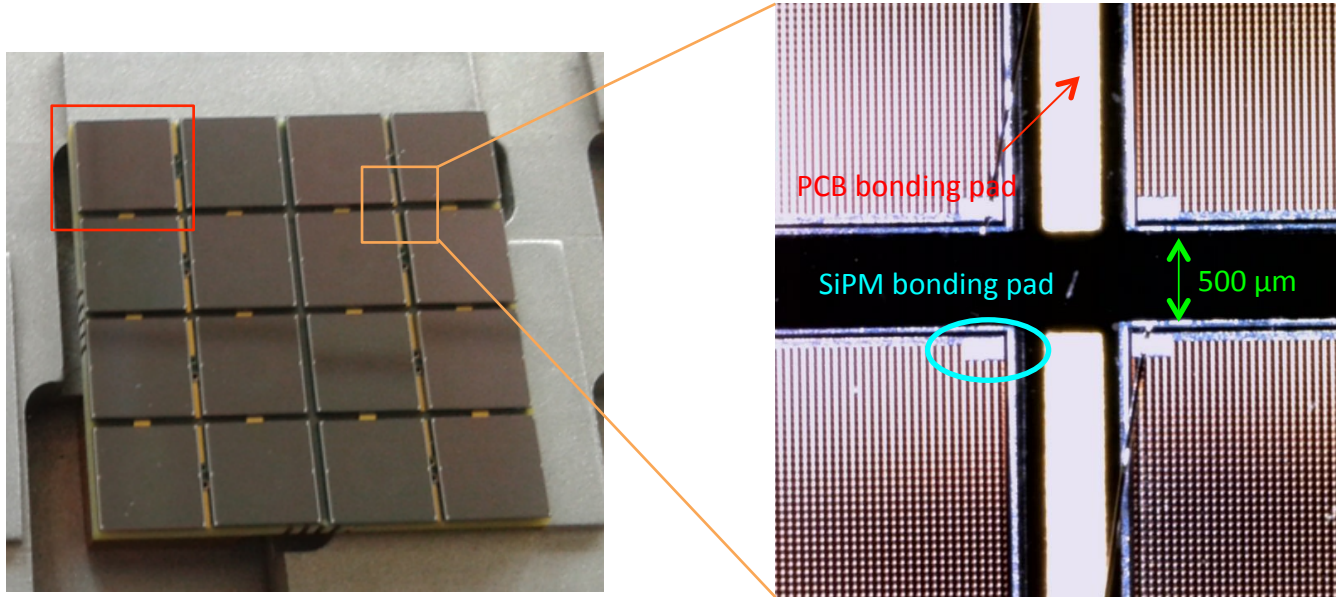


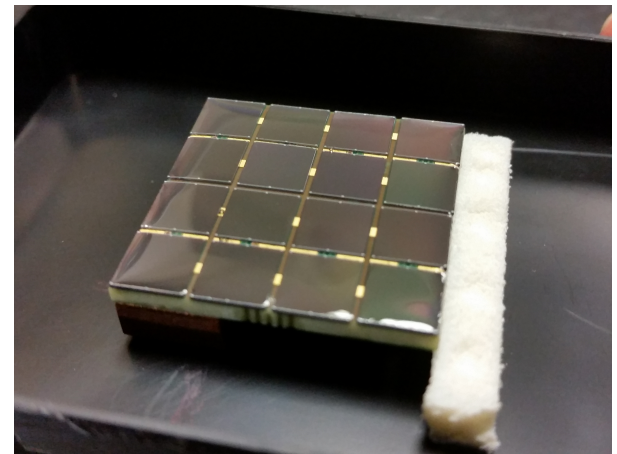
Figure 6, Oscilloscope shot showing the discrete nature of the SiPM output when illuminated by brief pulses of low-level light.

CTA SiPM Camera

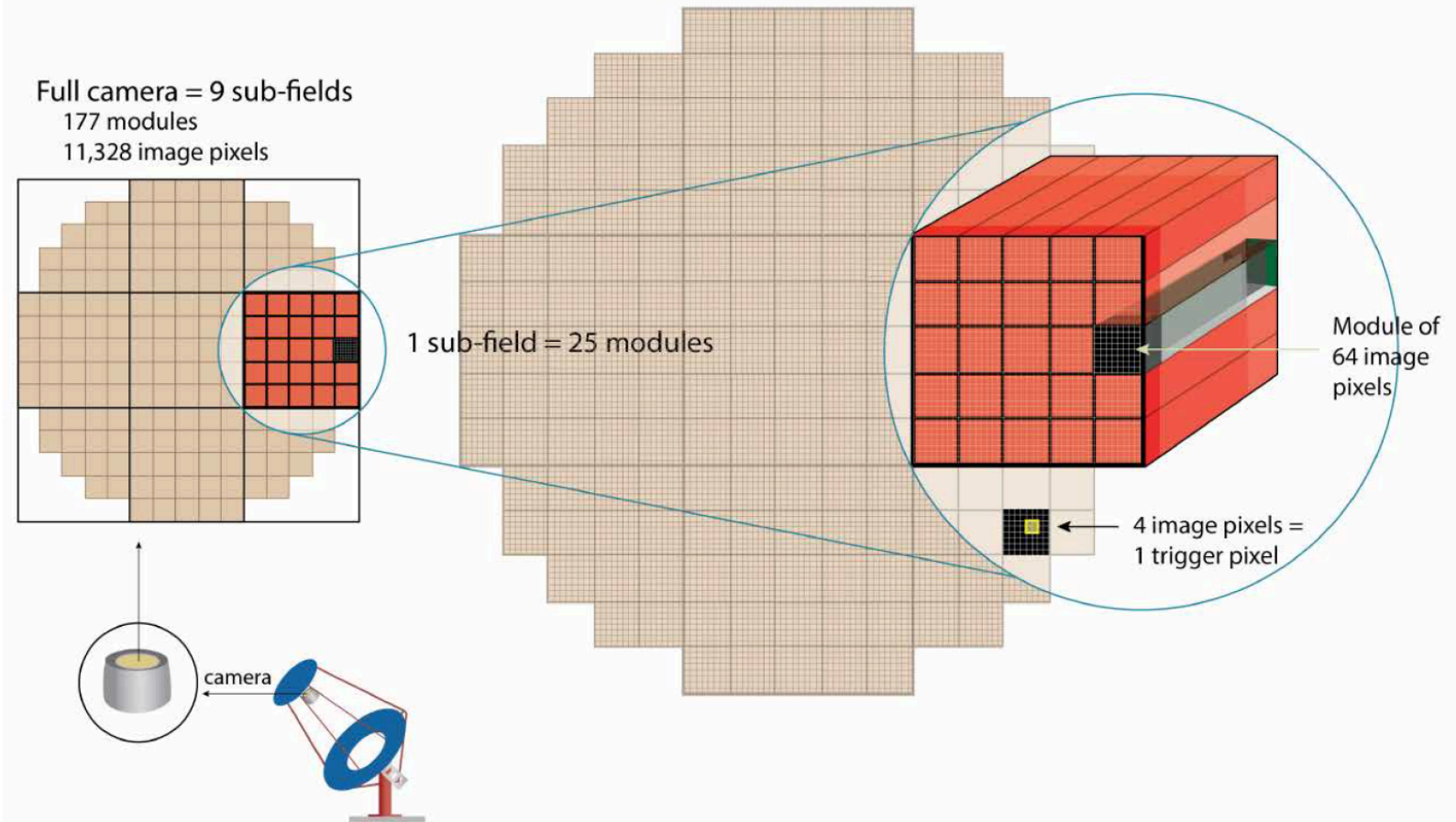


A camera prototype for a Medium Size CTA telescope is being developed in Perugia

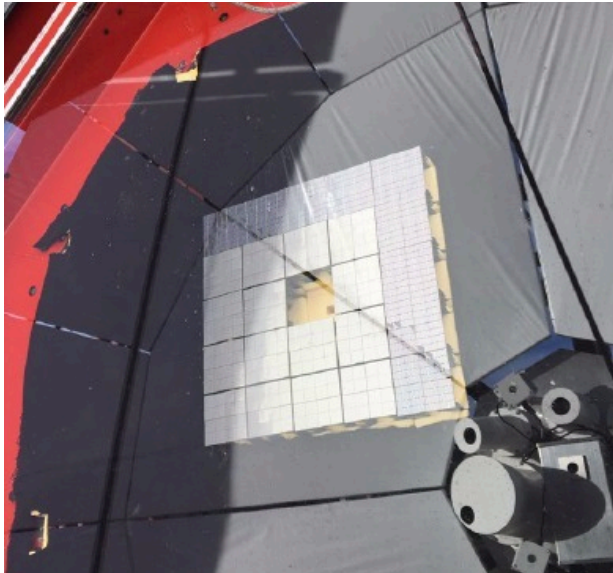
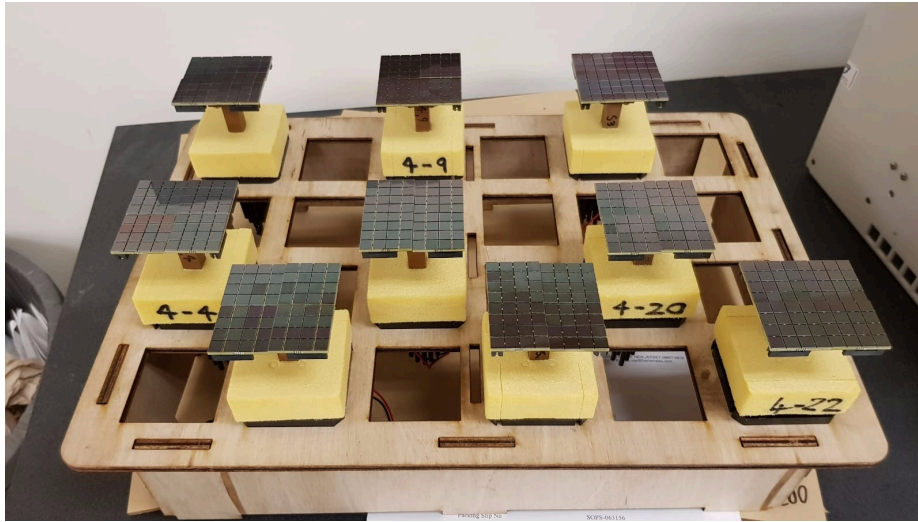
1 SiPM = 1 pixel of the camera



CTA SiPM Camera



CTA SiPM Camera



SCT telescope prototype, Arizona (US)